

Insights into the behaviour of biomolecules on the early Earth: The concentration of aspartate by layered double hydroxide minerals

Brian Grégoire, Valentina Erastova,
Dawn L.Geatches, Stewart J.Clark,
H.Christopher Greenwell and Donald G.Fraser

Published version information

Citation: B Grégoire et al. "Insights into the behaviour of biomolecules on the early Earth: The concentration of aspartate by layered double hydroxide minerals." *Geochimica et Cosmochimica Acta*, vol. 176 (2016): 239-258.

DOI: [10.1016/j.gca.2015.12.026](https://doi.org/10.1016/j.gca.2015.12.026)

©2016. This manuscript version is made available under the [CC-BY-NC-ND](https://creativecommons.org/licenses/by-nc-nd/4.0/) 4.0 Licence.

This version is made available in accordance with publisher policies. Please cite only the published version using the reference above. This is the citation assigned by the publisher at the time of issuing the AAM. Please check the publisher's website for any updates.

1 Mineral Concentration of Amino Acids on the Early Earth: Aspartate - 2 Layered Double Hydroxide Minerals

3 Brian Grégoire^{a#}, Valentina Erastova^{b#}, Dawn L. Geatches^c, Stewart J. Clark^d, H. Christopher
4 Greenwell^{b*}, Donald G. Fraser^a.

5 ^aDepartment of Earth Sciences, University of Oxford, South Parks Road, Oxford, OX1 3AN,
6 UK

7 ^bDepartment of Earth Sciences, Durham University, South Road, Durham, DH1 3LE, UK

8 ^c Daresbury Laboratory (STFC), Warrington, WA4 4AD, UK

9 ^dDepartment of Physics, Durham University, South Road, Durham, DH1 3LE, UK

10 [#]co-first authors

11

12 * Corresponding author: E-mail: chris.greenwell@durham.ac.uk

13 Abstract

14 The role of mineral surfaces in concentrating and facilitating the polymerisation of simple
15 protobiomolecules during the Hadean and Archean has been the subject of much research in
16 order to constrain the conditions that may have led to the origin of life on early Earth. Here
17 we examine the adsorption of the amino acid aspartate on layered double hydroxide minerals,
18 and use a combined computer simulation – experimental spectroscopy approach to gain
19 insight into the resulting structures of the host-aspartate material. We show that the uptake of
20 aspartate occurs in alkaline solution by anion exchange of the dianion form of aspartate,
21 rather than by surface adsorption. Anion exchange only occurs at values of pH where a
22 significant population of aspartate has the amino group deprotonated, and is then highly
23 efficient up to the mineral anion exchange capacity.

24

25 **1. Introduction**

26 Since Bernal first suggested some seventy years ago that minerals such as aluminosilicate
27 clays could have played an important role in the origin of life (Bernal, 1949), a wide range of
28 experiments has been undertaken to understand the structure and reactivity of simple
29 protobiomolecules and biomolecules at mineral surfaces (Hazen and Sverjensky, 2010), and
30 whether permutations of minerals, reaction conditions and environments could constrain the
31 search for the origin of life on Earth (Mejias *et al.*, 1999). Assuming that a legacy of those
32 original biomolecules remains within cellular make up, and that once evolved, the main
33 functional units of information transfer were determined, the search for the origin of life on
34 Earth has centred around the formation of either the first nucleic acid sequences (Powner *et*
35 *al.*, 2009) or the first proteins (Rode 1999).

36 Recent work shows that nucleic acid precursors, lipids and amino acids can all be
37 plausibly created on an early Earth (Patel *et al.*, 2015), and the RNA World has proved to be a
38 resilient hypothesis for the journey from geochemistry to biochemistry (Gilbert, 1986;
39 Hernandez and Piccirilli, 2013). On the other hand the presence of all known biogenic amino
40 acids in meteorites, as well as the ready availability of amino acids via abiotic Strecker and
41 Miller-Urey synthesis, suggests the “protein first” scenario is also a relevant and plausible
42 alternative hypothesis (Fitz *et al.*, 2007) and the abiotic generation of oligopeptides is of
43 importance, in any case. With the presence of the amino acid building blocks on the early
44 Earth and elsewhere seemingly indisputable, the generation of peptides requires a process of
45 concentration and subsequent condensation to form peptide bonds and this has been studied
46 by numerous researchers over the years, see (Lambert, 2008) for a recent review.

47 An elegant route for achieving amino acid concentration and peptide bond formation
48 has been via dense salt brines, used as experimental analogues for early Earth marine
49 evaporites. In brines, peptide-forming dehydration reactions occur naturally. Once the

50 concentration of sodium ions becomes high enough, their inner hydration spheres are lost.
51 The enthalpy of re-hydration of the sodium is then favourable enough to drive peptide bond
52 formation via a condensation reaction to re-establish the sodium hydration sphere. This is
53 named the salt induced peptide formation (SIPF) reaction (Schwendinger and Rode, 1992).
54 The addition of trace copper (II) ions to the brine leads to a preferential chelation
55 configuration by two amino acids and, hence, regio-selectivity in subsequent peptide forming
56 reactions (Plankensteiner *et al.*, 2004). Other studies have probed the role of heterogeneous
57 catalysts, especially those plausible on the early Earth. Notably, the possible roles of mineral
58 surfaces in protecting, selecting, concentrating, templating and catalysing reactions of
59 prebiotic organic molecules are recurrent themes in discussions of life's origins. The
60 adsorption of amino acids has been studied on a variety of minerals, including alumina
61 (Basiuk and Sainz-Rojas, 2001), silica (Bujdák and Rode, 1997; Martra *et al.*, 2014) and
62 aluminosilicate cationic clays (Bujdak *et al.*, 1994; Fraser *et al.*, 2011; Fraser *et al.*, 2011).
63 Some of these studies have also been undertaken on specific chiral surfaces of minerals in
64 order to shed light on both the polymerisation of amino acids, and the origin of homochirality
65 (Hashizume *et al.*, 2002). Layered minerals, such as clay minerals, are advantageous for
66 adsorption of protobiomolecules owing to their high surface area, permanent charge and ion
67 exchange capability, and the protecting environment between each 2-dimensional layer.

68 Layered double hydroxides (LDHs) form a class of naturally occurring and synthetic
69 anionic clays, with the most important group of these materials described by the general
70 formula $[M^{II}_{1-x}M^{III}_x(OH)_2] (A^{n-})_{x/n} \cdot mH_2O$, where M^{II} and M^{III} are di- and trivalent cations of
71 similar radii, respectively, A^{n-} is an exchangeable interlayer anion with charge n , and x
72 represents the $M^{II}/(M^{III}+M^{II})$ mole fraction (see **Figure 1**). Owing to their readily varied
73 compositions, anion-exchange properties, surface area and acid/base nature, these materials

74 are attractive for a wide range of materials science applications (Duan and Evans, 2006;
75 Grégoire *et al.*, 2012).

76 In previous work, amino acid-intercalated LDH systems have been prepared either by
77 direct co-precipitation of the mineral in the presence of amino acids, or via a reconstruction
78 route, where a mixed metal oxide precursor is rehydrated in the presence of the amino acid
79 (Fudala *et al.*, 1999; Pálinkó, 2006; Whilton *et al.*, 1997). However in the context of prebiotic
80 chemistry, the ability of an inorganic LDH to exchange a more labile simple inorganic anion,
81 for example chloride or sulphate, with an organic anion such as an amino acid (see **Figure 1**),
82 would have been key to concentrating biomolecules from dilute solutions and it is this
83 exchange that is the subject of the present paper.

84 It has been suggested that large quantities of mixed valence iron LDH minerals were
85 the precursors of banded iron formations (Lascelles, 2007) and, as such, the role of these
86 materials in concentrating biomolecules could have been significant. Other than in the
87 seminal work of Arrhenius and co-workers (Arrhenius, 2003; Kuma *et al.*, 1989), few papers
88 have looked at the role of anion exchange in layered double hydroxides in the context of
89 prebiotic chemistry. As with vermiculite gels (Fraser *et al.* 2011), the nano-sized interlayer
90 domain of LDHs provides a “nanoreactor” for confining reactants in a preferred orientation,
91 controlling the regio- and stereo-selectivity of products. Hybrid LDH materials with
92 intercalated amino acids or peptides have been explored for a variety of applications. For
93 example, Hibino investigated the delamination behaviour of LDH sheets for use in polymer
94 composites as a function of the nature of the intercalated amino acids (Hibino, 2004), while
95 Chen *et al.* studied the kinetics of oxidation of cysteine in a restricted environment provided
96 by the interlayer domain of LDH (Chen *et al.*, 2009). Demonstrating the added stability of
97 intercalated biomolecules, Wei *et al.* found intercalation of enantio-pure L-Tyrosine

98 prevented racemisation occurring when the materials were exposed to sunlight, or high
99 temperature (Wei *et al.*, 2005).

100 Despite their utility, LDH and other layered minerals present a challenge to structural
101 analysis, because the interlayer domain is dynamic at room temperature and hydrated at
102 atmospheric humidity, and the materials invariably have long-range order only in terms of the
103 stacking of the layers. Computational chemistry methods have become an essential adjunct to
104 experimental techniques for probing the structure and dynamics of intercalated molecules in
105 layered minerals (Newman *et al.*, 1998). A number of studies of hydrated intercalated layered
106 minerals have been performed using molecular dynamics (MD), including, for example, the
107 interactions of mono-, di- and trivalent carboxylate anions, including amino acids within LDH
108 interlayers (Greenwell *et al.*, 2006; Kalinichev *et al.*, 2010; Kumar *et al.*, 2006; Kumar *et al.*,
109 2007; Pisson *et al.*, 2011). These studies have highlighted the differences in interlayer water
110 interactions with inorganic and organic anions. Computational quantum mechanics studies
111 can provide detailed information about specific molecular interactions in mineral interlayer
112 environments (Aimoz *et al.*, 2012; Boulet *et al.*, 2006). Quantum chemistry methods have
113 also been used to study reactivity of peptides at mineral surfaces (Rimola *et al.*, 2007), and
114 this area has recently been reviewed by Coveney *et al.* (Coveney *et al.*, 2012).

115 In order that studies are relevant to the origin of life, realistic geochemical constraints
116 must be set. Since the discovery of the Lost City hydrothermal field (LCHF), the idea that life
117 originates in alkaline media has emerged (Baross and Hoffman, 1985; Kelley *et al.*, 2001;
118 Martin *et al.*, 2008). In these low temperature hydrothermal vents, reactions between seawater
119 and upper mantle peridotite produce methane and hydrogen-rich fluids that are highly alkaline
120 (pH 9 to 11). Hanczyc *et al.* demonstrated that physicochemical forces that are present in the
121 LCHF can drive the formation of vesicles and their division, strengthening the theory that
122 early life may have been cellular (Hanczyc *et al.*, 2003). Alkaline fluids also have many other

advantages; they favour phosphate and amine chemistry, and promote acid-base reactions, suitable for the formation of amino acids and a rich library of organic compounds (Ferris and Hagan Jr, 1984; Russell, 2003). From a mineralogical point of view, brucite ($\text{Mg}(\text{OH})_2$), formed during the convective hydration of rocks is expected to have existed on the early ocean floor (Schoonen *et al.*, 2004) and may have been abundant. The structure of LDHs derives directly from the brucite structure, and may result from weathering of Mg-rich and Al-rich minerals, and also from the formation of mixed valent Fe-rich minerals.

The nature of the interlayer anion in the LDH structure is also an important consideration. Owing to its symmetry and charge density, the carbonate anion is thermodynamically preferred and its presence in the interlayer domain prevents further anion exchange. In Archean sea water, atmospheric CO_2 and magmatic sources both contributed to the presence of carbonate species (predominantly bicarbonate or dissolved CO_2). In alkaline hydrothermal fluids, despite the elevated pH, the carbonate alkalinity is less than one third of sea water values because of the absence of a magmatic source (Kelley *et al.*, 2005). The elevated concentration of calcium further contributes to the removal of free carbonate anions from water, evidenced by the high quantity of calcite/aragonite minerals found at such locations resulting in carbonate chimneys 30 to 60 meters tall (Kelley *et al.*, 2001; Kelley *et al.*, 2005; Lang *et al.*, 2010; Martin *et al.*, 2008). The salinity of the early ocean is believed to have been 1.5 or 2 times that of today's ocean (Sleep, 2010), and therefore, chloride anions are likely to have been the most prevalent in the formation and stabilisation of LDH minerals near such hydrothermal fields. In the present study, we use experimental conditions indicative of these. The adsorption isotherms were carried out in the pH range of the hydrothermal field (pH 9 and 11) where we hypothesise LDH minerals may have been present in sufficient quantity to have played a significant role in the concentration of amino acids. Alkaline pH

further favours the presence of anionic amino acids with a deprotonated carboxylate group and deprotonated amino group suitable for their intercalation in the LDH galleries.

The present study brings together experimental methods and computational modelling to examine the exchange of aspartate (Asp) with chloride (Cl^-) within LDHs, and characterise the resultant organo-minerals. Aspartate was selected for this study because of its anionic nature due to its carboxylate side chain, and because it has been identified as one of the earlier amino acids to have been incorporated into biochemistry (Engel and Nagy, 1982; Hall *et al.*, 1971). By varying the pH of the external solution over a range of alkalinity, geochemical constraints can be placed on the exchange of amino acids, such as aspartate, into the mineral interlayer. Such alkaline conditions are considered to have been geochemically relevant at low temperature hydrothermal seeps (Baross and Hoffman, 1985). Importantly, the minerals used are redox-stable structural analogues of the green rust Fe(II)/Fe(III) LDHs thought to have been prevalent on the Archean Earth (Arrhenius, 2003).

2. Synthesis and Intercalation Methodology

Though it is possible to prepare $\text{Mg}_R\text{Al-Cl}$ (see definition below) LDHs directly via co-precipitation chemistry under an inert gas to prevent carbonate inclusion, it was decided to prepare $\text{Mg}_R\text{Al-CO}_3$ LDHs, and then exchange the carbonate for chloride using the procedure of Iyi *et al.* (Iyi *et al.*, 2011). This is more relevant to early Earth chemistry and delivers more uniform, larger crystal sizes than direct synthesis of the chloride containing LDH, thus facilitating reproducible adsorption isotherm measurements. All chemicals ($\text{MgCl}_2 \cdot 6\text{H}_2\text{O}$, $\text{AlCl}_3 \cdot 6\text{H}_2\text{O}$, 1M HCl solution, L-Aspartic acid, absolute ethanol, (ACS reagent grade) were provided by Sigma Aldrich and were used as supplied.

As this work includes materials with different composition, the following nomenclature was used through this manuscript. $\text{Mg}_R\text{Al-X}$ refers to LDH materials composed

of Mg and Al cations whose proportions are expressed by the value, $R = n(\text{Mg})/n(\text{Al})$. X represents the interlayer anions, namely, CO_3^{2-} , Cl^- or $\text{Asp}^{-/2-}$ (for aspartate) in this study. If the R value or X is not explicitly stated, we refer to generic LDH materials with any R value or X anions.

2.1. Chloride-layered double hydroxide preparation

A 0.4 M solution of MgCl_2 and AlCl_3 salts dissolved in water, with $\text{Mg}:\text{Al} = 2:1$ or $3:1$, was added slowly (0.3 mL/min) to a solution of Na_2CO_3 (0.25 M). The pH was kept at 11 by simultaneous addition of NaOH (1 M) solution using an auto-titrator (with an error of approximately ± 0.05 pH units). After complete addition of the cation solution, the slurry was aged for 20 h at 25°C . The final white crystalline solids were washed repeatedly with deionised water and dried at 60°C overnight. The $\text{Mg}_R\text{Al}-\text{CO}_3$ was converted to $\text{Mg}_R\text{Al}-\text{Cl}$ by an exchange reaction according to the method proposed by Iyi *et al.* (Iyi *et al.*, 2011). An ethanolic solution was prepared by diluting a 1 M HCl solution in 5 mL of ethanol. This was slowly added to a vigorously stirred $\text{Mg}_R\text{Al}-\text{CO}_3$ suspension (0.662 mmol of $\text{Mg}_R\text{Al}-\text{CO}_3$ i.e. 161.3 mg and 199.9 mg for the ratio $R = 2$ and 3, respectively) in 45 mL ethanol solution under nitrogen flow. The factor f , defined by Iyi *et al.* as $f = [\text{HX}] / (2 \times [\text{CO}_3^{2-}])$ where $[\text{HX}]$ represents the monoprotic acid concentration, was set to 1.5. The suspension was stirred for 1 h at room temperature under N_2 . The suspension was filtered with a polycarbonate membrane (0.2 μm), and the solid washed thoroughly with absolute ethanol and dried at 60°C . The elemental composition of these LDH phases is reported in **Table A1 (SI)**.

2.2. Adsorption isotherm experiments

To avoid carbonate contamination, adsorption isotherms were run in a glove box purged by N_2 , at 25°C and ultrapure water was boiled, purged with N_2 , and allowed to cool down to

room temperature. 0.2 mmol of $\text{Mg}_R\text{Al-Cl}$ (i.e. 48.0 mg and 59.7 mg based on the formula $\text{Mg}_2\text{Al}(\text{OH})_6(\text{Cl}) \cdot 1.5 \text{H}_2\text{O}$ and $\text{Mg}_3\text{Al}(\text{OH})_8(\text{Cl}) \cdot 1.5\text{H}_2\text{O}$ respectively) was added to a racemic solution of aspartic acid, with the aspartic acid concentration varied from 2 to 100 mmol/L. The pH was adjusted to either 9 or 11 by addition of a NaOH solution at 1 M. Each experiment was duplicated. To ensure equilibrium had been reached, the suspensions were stirred for 20 h. Finally, the white polycrystalline solid was separated by filtration.

2.3 Hydration state dependence of structure

Three relative humidity levels were considered: RH 0%, 25% and 88%. To achieve these, the LDH materials were initially placed for 48 h in an oven at 150°C. The LDH phases were removed from the oven and placed for a further 48 h in a desiccator filled with a 55% w/w solution of sulphuric acid, to produce a relative humidity of 25%, and then for 48 h with a solution of 20% w/w to give a relative humidity of 88%. After each step, the sample weights were measured allowing the determination of the interlayer water content. The formulae of the phases obtained are reported in **Table A6 (SI)**. For given interlayer water content, the samples were analysed by ATR-FTIR and XRD.

2.4. Mineral characterisation

Powder X-ray diffraction (XRD). Patterns were recorded with a Phillips X'Pert Pro MPD diffractometer in reflection geometry using $\text{Cu K}\alpha_1$ radiation ($\lambda = 1.5406 \text{ \AA}$). Samples were finely ground and continuously rotated to improve statistics. The 2θ range was between 5–70° with a step size of 0.01671° and a scan time per step set at 2s giving a scan rate of 2°/min. In order to make the determination of the cell parameters easier, the XRD lines were fitted with Lorentzians. The fitting was made with the minimum number of Lorentzians per XRD peak needed to obtain a regression coefficient better than 0.99.

Fourier Transform Infra-Red (FTIR) Spectroscopy. FTIR spectra of solution or samples at different relative humidity were acquired on a Varian FTS-7000 spectrometer equipped with a diamond attenuated total reflectance (ATR) cell. A KBr beamsplitter and a deuterated tryglycine sulphate (DTGS) detector were used to perform the analysis. For liquid, a 0.1M aspartate solution was prepared. Intensities were then corrected to reflect the real concentration after dilution with HCl or NaOH to obtain different pH values. Solids were analysed on their own, without any specific preparation. The spectra were acquired with a resolution of 4 cm^{-1} and 100 acquisitions were averaged per sample.

Elemental analysis. The Mg:Al ratio of the synthesised and exchanged LDH was determined by inductive coupled plasma - atomic emission spectrometry (ICP-AES) on an Ultima apparatus (Jobin Yvon). Prior to measurement, the LDH materials were dissolved in a 2 M HNO_3 solution and the solution filtered before analysis.

2.5. Adsorption isotherm analysis

After the LDH mineral had been in contact with the aspartate solution for 20 h, the amino acid solution was filtered and analysed by high performance liquid chromatography (HPLC) to quantify the amount of amino acid adsorbed. A chiral column was used to measure the L to D aspartate isomer ratio in solution to study any enantioselectivity. The stock aspartate solutions served as standards. All runs were made in duplicate and three analyses per run were averaged. Two μl of the sample were injected into a Phenomenex Chirex 3126 (D)-penicillamine LC column (150 x 4.6 mm), equipped with a 15 mm guard column. Analysis was performed in the isocratic mode with a mobile phase consisting of 85% of a 2 mM CuCl_2 solution and 15% of methanol, pumped at 1 ml/min. The calculated separation factor, α , using

these conditions is 1.42. The limit of detection based on this method was calculated from the regression curve and was found to be 1.06 mmol/L.

3. Computational Simulation Methodology

To investigate the structure and properties of the interlayer region in more detail we have used a combination of quantum mechanical, periodic, density functional theory (DFT) calculations and molecular dynamics (MD) simulations.

3.1. Quantum mechanical calculations

Model structures of the Mg_RAl-Asp systems were constructed and the energy of each model was iteratively minimised through adjustment of its atomic coordinates and calculating the total energy using DFT. As DFT is computationally demanding, and the intercalated LDH models were relatively large (between 150 to 400 atoms) and lacking in symmetry that would otherwise speed-up such calculations (by enabling a reduction in the number of k-points used to sample the Brillouin zone, for example) the total number of models investigated was constrained to those described as follows.

3.1.1. Model Construction

The initial structures were based on the magnesium hydroxide (Mg(OH)₂) mineral brucite. LDH models were created with the formulae [Mg₂Al(OH)₆]⁺ and [Mg₃Al(OH)₈]⁺, respectively. Each model contained two interlayer regions, with enough aspartate amino acids to balance the layer charge. Each periodic model contained two interlayer's (see **Figure A1, SI**) and all simulation cell angles and lengths were free to vary.

Aspartate Models. Within the simulations, pH was taken into account by changing the protonation state, and thus charge, on the aspartate, -1 was applied for aspartate at pH below the pKa of the amine group (pKa = 9.6) and -2 for pH higher than the pKa of the amine group.

Mg₂Al LDH Models. Supercells were prepared with formulae [Mg₂₄Al₁₂(OH)₇₂].(C₆H₇O₇N₂)₆ and [Mg₂₄Al₁₂(OH)₇₂].(C₆H₇O₇N₂)₁₂. All aspartates were initially orientated with the long axes, defined as being between the two carboxylate groups, perpendicular to the LDH layers (as shown in **Figure A1a, SI**). The model containing the aspartates with charge -1 reached a plateau in its geometrical minimisation, and had difficulty in achieving atomic force convergence at lower than 0.05 eV/Å. This indicated that the force convergence criteria imposed on it were artificially too tight. The total energy of this model was converged to 10⁻⁵ eV, matching the total energy convergence of all other models and therefore the results are comparable.

Mg₃Al LDH Models. The supercell had a formula of [Mg₂₄Al₈(OH)₆₄].(C₆H₇O₇N₂)₄. A number of aspartate starting configurations were assembled in order to reduce the possible configurational bias, which is larger at lower LDH charge density owing to there being more space per amino acid to sample (see **Table A2, SI**).

Hydration states. To investigate the effect of intercalated water on the geometry of the interlayer, aspartate models were set up with: no water, two waters per aspartate and five waters per aspartate. The water molecules were placed with an approximately uniform spread around the aspartates without a pre-defined orientation (**Table A2, SI** collates the full information of the model set up, including the labelling of the models that will be used from this point onwards).

3.1.2 Density Functional Theory Simulation Methodology

DFT calculations were carried out using CASTEP (Clark *et al.*, 2005), a plane-wave pseudopotential DFT code. Plane-waves are particularly suited as the basis set for periodic models.

Choice of pseudopotential. The pseudopotentials represent the ion-electron interactions, and their choice depends on a number of factors, for example, accurate, simulated spectroscopy demands pseudopotentials with ‘hard’ cores (Martin, 2004), whereas structural relaxations are equally amenable to ‘hard’ or ‘soft’ i.e. ultrasoft pseudopotentials. Both types of pseudopotentials were employed in the study, norm-conserving for the LDH with $R = 2$ (Lee, 1996), and ultrasoft (Vanderbilt, 1990) for the LDH with $R = 3$. Also, one system ($[\text{Mg}_2\text{Al}(\text{OH})_6]^+0.5\text{Asp} \cdot 2\text{H}_2\text{O}$) was simulated with both potentials to assess the effect of pseudopotential type. The pseudopotential determines the size of the basis set required for the expansion of the valence electron wavefunctions; these were represented by 550 eV for the LDH with $R = 2$ and 380 eV for the LDH with $R = 3$, both of which achieved energy convergence tolerances to better than 1 meV per atom. The Brillouin zone integrations (commonly known as k-point sampling) were performed on variously sized Monkhorst-Pack grids (Monkhorst and Pack, 1976), according to the size of the models. All geometries (except for Mg_2Al containing aspartates of charge -1) achieved the same force tolerance criteria of 0.03 eV/Å.

Choice of functional. The exchange and correlation effects were treated with the generalised gradient approximation (GGA) of Perdew Burke and Ernzerhof (PBE) (Perdew *et al.*, 1996), as this is more suitable for molecular bonding than the local density approximation.

Optimisation method. The electronic energy was minimised using density mixing and the total atomic energy using the Broyden-Fletcher-Goldfarb-Shanno (BFGS) algorithm (Head and Zerner, 1985), based on the reduction of forces acting on the nuclei, under which all unit cells and all ions were allowed to relax to their geometrical equilibria. In a study by Ugliengo *et al.* it was demonstrated that inclusion of dispersive forces was important when studying LDH materials (Ugliengo *et al.*, 2009). Van der Waals forces were applied via the DFT semi-empirical dispersion interaction correction (DFT-SEDC) (McNellis *et al.*, 2009), specifically Grimme 06 (Grimme, 2006). The following convergence criteria were used for all models (unless otherwise stated): electronic energy: 1×10^{-7} eV; total energy: 1×10^{-5} eV/ion, and all calculations were non-spin polarised.

3.1.3 Density Functional Theory Simulation Analysis

Structural properties. Simulated powder X-ray diffraction patterns (XRD) were created from the equilibrated models using the Reflex module within Materials Studio (Accelrys, 2012). The simulated radiation sources were $\text{Cu}_{\alpha 1}$; the diffractometer range was 2θ from 5° to 70° ; the temperature factor was atomic and the line shift Bragg-Brentano. Neither asymmetry-correction nor any lattice strain was applied. The simulated structure XRD diffraction patterns, calculated interlayer spacings, and snapshots of the final optimised structures are in the supplementary information (**Table A3** and **Figure A3** to **Figure A14, SI**).

Atomic charge calculations. Following full relaxation of the lattice and ions to the convergence criteria described above, the charge density of the models was analysed using Mulliken population analysis (Mulliken, 1955; Mulliken, 1955; Mulliken, 1955; Mulliken, 1955), which in CASTEP is implemented by first projecting the plane wave states onto a localised basis (Sanchez-Portal *et al.*, 1995), followed by analysing these projected states

under the Mulliken formalism to produce a population analysis. Mulliken analysis is particularly useful for identifying trends in consistently-parameterised systems (Segall *et al.*, 1996; Segall *et al.*, 1996) rather than for calculating absolute charges due to its sensitivity to the atomic basis set (Davidson and Chakravorty, 1992). The calculated atomic charges were used to adapt the ClayFF force field (Cygan *et al.*, 2004) parameters, as described in Section 3.2.2 and are given in **Table A4, SI**.

3.2 Molecular Dynamics Simulations

To provide further understanding of the structure of the Mg₃Al-Asp LDHs, classical molecular dynamics (MD) simulations were undertaken on these systems, enabling models of greater size, and more representative statistics of the thermally induced dynamics of these systems to be obtained.

3.2.1. Model construction

The model used for MD simulations was based upon the LDH layer coordinates for the Mg₃Al-Asp used in the DFT simulations and is shown in **Figure A2, SI**. The initial step was to create a Mg₃Al LDH surface of 114.56 Å x 110.24 Å. 180 randomly distributed aspartate amino acids, deprotonated at both carboxylic groups (2-) were inserted. The resulting layer was solvated with 20 water molecules per aspartate, totalling 3600 molecules per layer. The layer was replicated 5 times along the crystallographic *c* parameter. Further hydration states were formed through decreasing the number of water molecules, as discussed below.

3.2.2 Force field selection

The ClayFF force field (Cygan *et al.*, 2004) was used in this work to model the Mg₃Al-Asp LDH. The charges of the Mg₃Al-Asp LDH were slightly altered from the original ClayFF to

add up to an integer of 1 per unit cell, charges are given in **Table A5 (SI)**. Mulliken charges were assigned from the DFT calculations. Aspartate was modelled with the CHARMM27 force field (MacKerell *et al.*, 2000), designed for amino acids and compatible with ClayFF (Underwood *et al.*, 2015). Simple point charge (SPC) water was used (Berendsen *et al.*, 1981). Both force fields use Lorentz-Berthelot mixing rules for Lennard-Jones interactions.

3.2.3 Molecular Dynamics Simulation Protocol

All molecular dynamics simulations were performed using GROMACS 4.6.2 (Hess *et al.*, 2008) software, using a 14 Å cut-off for both Columbic and Lennard-Jones interactions and using periodic boundary conditions in x, y, z directions. After set up the simulation was first energy minimized to remove any high forces. A steepest descent algorithm and force tolerance of 100 kJ/mol/nm per atom was used. MD simulations were run for 1 ns with a 1 fs time-step at a constant temperature of 300 K and a pressure of 1 bar, using the Berendsen thermostat and barostat. Equilibration occurred within the first 100 ps. When the first system with 20 waters per aspartate was equilibrated, 5 water molecules per aspartate were removed, leading to a new model of 15 water molecules per aspartate that was energy minimised again, and equilibrated. By this method a set of simulations with varying degrees of hydration: 20, 15, 10, 7, 5, 3, 2 water molecules per aspartate and a dehydrated system were obtained.

3.2.4 Molecular Dynamics Visualisation and Analysis

All images were produced with VMD 1.9.2 (Humphrey *et al.*, 1996). The LDH layer near the bottom/top of the periodic cell was shown on both sides of the visualised cell. The data from the trajectory was extracted with the Tcl (tool command language) scripts in VMD and further analysed with Python 2.7 codes developed by the authors. Graphs were plotted using XMGrace.

4. Results

4.1. Characterisation of Layered Double Hydroxides

The X-ray diffraction patterns of the $\text{Mg}_R\text{Al-Cl}$ and $\text{Mg}_R\text{Al-CO}_3$ LDHs prepared are shown in **Figure 2a** and **2b**. The patterns are characteristic of LDH minerals, with basal reflections observed below $30^\circ 2\theta$. The $\text{Mg}_R\text{Al-CO}_3$ LDH shows characteristic sharp reflections for both R ratios, indicating a crystalline sample with a characteristic interlayer spacing of 7.67 Å and 7.81 Å for the $\text{Mg}_2\text{Al-CO}_3$ and $\text{Mg}_3\text{Al-CO}_3$ LDH samples respectively, in good agreement with previously reported refined structures for these minerals (Hofmeister and Platen, 1992). The cell *a*-parameter can be used as an indicator of the Mg:Al ratio owing to the difference in ionic radii between Mg and Al, and was found to be 3.044 Å and 3.068 Å for $\text{Mg}_2\text{Al-X}$ and $\text{Mg}_3\text{Al-X}$ ($X = \text{CO}_3$ or Cl), in good agreement with literature values (Bellotto *et al.*, 1996; Grégoire *et al.*, 2012; Richardson, 2013) confirming the relative proportions of layer cations reflected the reactants. The Mg:Al ratio determined from ICP-AES agreed well with the quantity of Mg^{2+} and Al^{3+} salt initially added in solution to synthesise the material, and this was not observed to change during subsequent exchange processes. Exchange of carbonate by chloride resulted in expansion of the interlayer space to 7.80 Å and 7.96 Å for the $\text{Mg}_2\text{Al-Cl}$ and $\text{Mg}_3\text{Al-Cl}$ samples, respectively, owing to the way that the chloride anion sits between the hydroxide sheets (Hines *et al.*, 2000; Trave *et al.*, 2002). FTIR results show the presence of carbonate vibrational bands at 1365 and 1377 cm^{-1} for $\text{Mg}_2\text{Al-CO}_3$ and $\text{Mg}_3\text{Al-CO}_3$, respectively. These bands were absent in the FTIR spectra of the $\text{Mg}_R\text{Al-Cl}$ phases, confirming that the exchange was complete.

4.2. Aspartate Exchange and Adsorption by Chloride Layered Double Hydroxide

Figure 3 shows the adsorption isotherms for exchange of aspartate with chloride in the LDHs. In **Figure 3a**, the $\text{Mg}_2\text{Al-Cl}$ LDH system shows a typical Langmuir isotherm. After 20 h, a high concentration factor of aspartate is shown even from very dilute solutions (20 mmol/L) to give an interlayer concentration of approximately 7.93 mol/L with a hydration state of 26% H_2O by mass (corresponding to 7 mol H_2O / mol Asp). The Langmuir isotherm reaches a plateau at the maximum anion exchange capacity of 0.5 mol Asp / mol Al, indicating that all chloride has been exchanged and that the intercalated aspartate is all present with a charge of 2-. Further adsorption isotherms were also performed at pH 7 for both LDHs, but no intercalation of amino acid was observed. The adsorption isotherms at pH 9 and 11, displayed in **Figure 3a**, exhibit very similar profiles with a plateau corresponding to the occupation of half of the interlayer sites, presumably because of the preferred intercalation of Asp^{2-} over Asp^{-1} . The adsorption isotherm of $\text{Mg}_3\text{Al-Cl}$ LDH, displayed in **Figure 3b**, exhibits distinctive features since the maximum of adsorption is reached at a much higher initial solution concentration of aspartate ($C_0 = 100$ mmol/L).

4.3. Characterisation of the Aspartate Intercalated Layered Double Hydroxide

ATR-FTIR spectra of aspartate solution at different pH were obtained in order to identify the protonation state of the intercalated amino acid as well as the binding conformation of the aspartate molecule (**Figure 4a**). Spectra recorded at pH 7 and pH 9 present very similar features, due to the presence of protonated amino- and deprotonated carboxylate-groups. The large bands at 1587 cm^{-1} and the bands at 1414 (shoulder)/ 1394 cm^{-1} are attributed to the anti-symmetric stretching and the symmetric stretching of the carboxyl group. The presence of large bands or shoulders may indicate the contribution of the two carboxyl groups and seems to be coupled with the amino bending modes. The band at 1476 cm^{-1} is attributed to the symmetric bending mode of the $-\text{NH}_3^+$ moieties. Below 1394 cm^{-1} , modes arise from CH_2

(wagging and bending modes) and C-N, C-O and C-C modes (Wolpert and Hellwig, 2006). Distinct changes are observed when the pH is increased to 11. At such a high pH, the aspartate molecules are expected to be fully deprotonated and experimentally, the band at 1476 cm^{-1} is observed to disappear completely. Interestingly, the anti-symmetric bands shift to 1557 cm^{-1} and get narrower while the symmetric stretch remains unchanged at 1396 cm^{-1} and becomes more symmetrical. The two carboxyl groups of the molecules are thus no longer distinguishable.

Note that the observed FT-IR spectra of intercalated aspartate are very similar to the aqueous aspartate spectra (**Figure 4b**). The carboxyl modes have peaks at 1554 cm^{-1} and 1400 cm^{-1} , while the distinct vibrational mode of the $-\text{NH}_3$ group expected at 1476 cm^{-1} is completely absent. This suggests that the amino acid is deprotonated. This result is in good agreement with the adsorption isotherm that showed that only half of the interlayer sites to be occupied by amino acids.

4.4. DFT study on Mg_2Al Layered Double Hydroxides

All of the optimised Asp- Mg_2Al model structures and their simulated XRD patterns are in **Figures A3 to A14, SI**. The interlayer space and the energies of the optimised models are given in the **Table A3, SI**.

4.4.1 Effect of aspartate charge on interlayer structure.

The dependency of the pH (charge of aspartate) on the interaction of aspartate with LDH can be observed. When aspartate is present with -1 charge, a bilayer or mixed/interdigitated bilayer is formed in the interlayer, with a calculated interlayer spacing of 15.54 Å. At higher pH, aspartate carries a 2- charge and, as such, requires fewer molecules to counterbalance the LDH layer charge, in which case the aspartate molecules form a monolayer with an interlayer

spacing of 8.27 Å, bridging across the interlayer with opposing carboxylate groups on each amino acid.

4.4.2 *Effect of hydration state on interlayer structure*

Hydration state is variable in layered double hydroxides, depending on the nature of the interlayer, and the ambient humidity. The amount of water in the interlayer region influences the orientation of the other anions present (Newman *et al.*, 1998). With the increase of the hydration the increase in the interlayer spacing is observed to change from 3 Å (Mg₂Al) and 3.8 Å (Mg₃Al) with no interlayer water, to 4.9 Å (Mg₂Al) and 6.2 Å (Mg₃Al) with 5 waters per aspartate hydration. As the hydration state increases the aspartate molecule rotates from co-planar to the layers to approximately 45° to the layers. When aspartate is co-planar, on some of the aspartates the oxygen atoms on the same carboxylate group bridge to opposite sides of the interlayer, but as hydration increases, the carboxylate groups on each amino acid bind to one layer only, bridging with the second carboxylate group to the other layer. These changes are evident for both Mg₂Al and Mg₃Al systems in **Figure 7**.

4.4.3. *Effect of initial orientation of aspartate on interlayer configuration*

Owing to the confining nature of the interlayer space, the presence of water and the high charge, coupled with strong hydrogen bonding, many local minima on the complex potential energy surface are encountered during optimisation of the LDH structures (Greenwell *et al.*, 2006). To counter this, in the present study the effect of the initial molecular arrangement on the final minimised geometry was investigated. An alternative route would be to run an annealing or molecular dynamics run with CASTEP of the models, where thermal motion is applied to the model systems, though these techniques consume large amounts of computational resources.

Four different starting interlayer arrangements of aspartate, with two waters per aspartate were optimised and, in all four cases, the system converged to within very similar energies with the differences circa 0.5×10^{-4} %. In all cases aspartates were observed to lie co-planar, with the long axis parallel to the LDH layers (see **Figures A8 - A11, SI** for the snapshots). The direction of the aspartate in the initial model was not observed to play an important role in the final arrangement. The computationally predicted interlayer spacing ranges from 3.81 Å to 3.95 Å. The small variations of the *d*-spacing between models of the same composition and different initial configurations demonstrates the slight dependence of the final configuration on the starting alignment.

4.5. Molecular Dynamics simulations of the effect of hydration on Layered Double Hydroxide structure.

To complement the experiments and DFT calculations, a variety of different hydration levels of aspartate - Mg₃Al systems were studied with larger-scale MD simulations. We considered hydration levels ranging from 20 to 0 water molecules per each charge-balancing aspartate. The simulated interlayer structures are displayed in **Figure 8**. Looking at the structures, slight undulations of the hydroxyl layer are observed that are even more prominent at high hydration levels. Such features are often observed in large-scale systems presenting 2-dimensional layers and may result from thermal activation (Thyveetil *et al.*, 2007). The basal spacings determined for all the systems are reported in **Table A7 (SI)**. The standard deviation reflects the small fluctuations of the simulation box, as well as undulations of the layer, and allows an estimate of the extent of the undulations as a function of the water content. It can be seen that generally the standard deviation is greater for more hydrated systems, where the layers are more dynamic. This effect most certainly results from the loosening of the electrostatic interactions between the positive layer and the interlayer amino acids, screened

by the water molecules. At up to 5 water molecules per aspartate the basal spacing is almost constant, before increasing gradually on further addition of water molecules.

In order to investigate the orientation of the amino acid within the interlayer gallery upon hydration, changes of the angle of the vectors assigned between (a) oxygens in sidechain carboxylic groups, (b) oxygens on the back-bone carboxylic groups and (c) between carboxylic carbons, were monitored with respect to the LDH surface (**Figure 9**). For the dehydrated system the vector between oxygen atoms is mainly perpendicular to the LDH, more so than for the carboxylic group of the backbone. While the basal spacing was not observed to change until 3 water molecules per aspartate were added, the sidechain – carboxylate groups underwent more pronounced conformational changes, while the $C\alpha - C\beta$ backbone orientation remained the same. Obvious changes of the orientation of the sidechain appear over a hydration level of 7 water molecules per aspartate, concomitant with the sudden increase of the basal spacing. The amino acids then attach only with one carboxylate to the surface of the LDH and become more mobile. However, the amino acid never reaches a completely vertical orientation for any hydration content.

The analysis of the partial density of the MD simulation boxes allows further insight into the distribution of the water within these phases. As observed in **Figure A15 (SI)**, at up to 5 water molecules per aspartate, the water molecules are located in almost the same plane as that occupied by the aspartate molecules.

Further analysis of the dynamics of the system was carried out, looking to pick out the aspartate orientations that could lead to α -peptide (**Figure 10a**) or β -peptide (**Figure 10b**) linkages. In this analysis, the closest carbon in a carboxylic group of a neighbouring molecule within 3.5 Å of a nitrogen atom was found. This means that these pairs can only be included in one of the two peptide-bond formation orientations. In a small number of configurations, two adjacent aspartate molecules may form two β -bonds leading to the formation of cyclic

molecules (**Figure 10c**), such orientations were excluded from the count. **Figure 11** shows the plot of the percentage of the pairs in either α -peptide or β -peptide orientations. Standard deviation on the graph corresponds to the fluctuation in pair numbers through the length of simulation. It is clear from this analysis that, as hydration drops below 7 water molecules per aspartate, amino acids find themselves significantly more likely to form peptide bonds, resulting in a total of 1/3 of all pairs at a reactive distance for 0-3 water molecules per aspartate.

5. Discussion

5.1. Uptake Mechanism of Aspartate by Chloride Layered Double Hydroxide Minerals.

LDH minerals are not stable with respect to dissolution below \sim pH 7 and relic deposits of natural LDH minerals on present day Earth are typically associated with alkaline hydrothermal systems. Any LDH minerals formed in this environment would then be stable across the hydrothermal fluid gradient, but susceptible to slow hydrolysis once hydrothermal activity ceased or the mineral deposit exceeded a certain distance from the vent system. On hydrolysis they would have released any concentrated/reacted molecules from within the interlayer. Conceptually, this latter step is critical as once reacted in the interlayer, for oligo- or polypeptides to become functional, they would need to be released, indicating why geochemical gradients are critical to early-Earth proto-biomolecule evolution (Martin and Russell, 2007).

To represent suitable geochemical pH gradients, adsorption isotherms were carried out at pH 7, 9 and 11. The results presented here show that the effect of pH was critical in allowing the successful intercalation and concentration of amino acids in LDHs. At pH 7, all amino acids present in solution have their amino group protonated and exist as zwitterions.

Electrostatic repulsion between the positive layer of the LDH and the amino acids in solution prevents either surface adsorption or anion exchange of chloride and no adsorption was observed. Interestingly, in previous work, NMR investigations showed that intercalated glutamate amino acids existed with -1 and -2 charges i.e. with some amino groups protonated (Reinholdt *et al.*, 2009). However, in this case, the LDH-amino acid samples were obtained by a co-precipitation route (high pH), whose mechanism of formation differs from the exchange reaction used here, though may be geochemically relevant in some early Earth hydrothermal systems. Similarly, Aisawa *et al.* observed that the intercalation of phenylalanine in a ZnAl LDH by a reconstruction method is preferred at pH 7 implying that the amino acid is especially present as a zwitterion (Aisawa *et al.*, 2004), though the very reactive metal oxide minerals in this approach are less relevant to early Earth scenarios.

At pH 9 and 11, for the Mg₂Al-LDH, the Langmuir isotherm plateaus at the maximum anion exchange capacity of 0.5 mol Asp / mol Al, shown in **Figure 3**, indicating that all the chloride has been exchanged (as Al/Cl = 1) and that the intercalated aspartates is all present with a charge of -2. The Mg₃Al-LDH isotherm, **Figure 3b**, also shows a maximum anion exchange capacity of 0.5 mol Asp/mol Al, though attained at higher initial solution concentrations of Asp. These results establish that the Asp is taken up by LDH-Cl minerals via an anion exchange process and not via surface/edge site adsorption, otherwise we would expect to see adsorption amounts above the anion exchange capacity, and the adsorption to be invariant of Mg/Al ratio. Furthermore, the concentration of amino acids by LDH-type minerals requires alkaline conditions to be present, as the protonated zwitterion amino carrying aspartate was not taken up at pH 7. This is explored further below.

At higher pH, the relative proportion of aspartate -1 (i.e. with a protonated amino group) to aspartate -1 anions can be calculated to be: pH 9 = 20.1% of Asp -2 and 79.9% of Asp -1; pH 11 = 96.2% of Asp -2 and 3.8% of Asp -1. It might therefore be expected that at

pH 9 significantly less amino acid would be removed from solution by the LDH mineral. In fact, the adsorption isotherms for both materials suggest that all the intercalated aspartate is present as Asp -2, even when the bulk solution pH was 9 (**Figure 3**). **Figure A1 (SI)** shows the calculated quantity of Asp -2 and Asp -1 available in solution at pH 9 versus the measured quantity of aspartate anions present in the LDH at maximum exchange. From the position of the two series of points representing the adsorption isotherms, it can be noted that for the same number of available interlayer sites and for a given initial concentration, twice as many anions are intercalated in the Mg_2Al , when compared to Mg_3Al LDHs.

It is likely that once Asp -2 is preferentially exchanged, depleting the solution Asp -2 concentration, the solution aspartate re-equilibrates to generate more Asp -2 thus maintaining the equilibrium ratio. The exchange reaction thus favours an increasing overall population of Asp -2 at lower pH than would normally be expected. This mechanism does not operate at pH 7, where no exchange is observed, owing to the negligible amount of Asp -2 present, though the effect appears to be cooperative and we speculate that once a non-negligible amount of Asp -2 is present a tipping point is reached, whereupon the uptake of some Asp -2 results in a positive feedback loop until all chloride exchange for Asp -2 is completed. Having established that the uptake of the Asp -2 results in complete exchange for chloride such that dilute solutions of aspartate may be concentrated to ~ 8 mol/L in the Mg_2Al -LDH, it would be prescient to understand the interlayer arrangement of the biomolecule-mineral hybrid formed.

5.2. The Interlayer Structure of $Mg_{2R}Al$ -Asp

The structure of the interlayer of 2-dimensional layered mineral systems, such as LDHs, is greatly affected by water content which varies according to the ambient relative humidity, it is therefore important to assess the effect of water content during the characterisation process.

Structure of Mg_2Al -Asp LDHs. The XRD pattern and the FTIR spectra of the Mg_2Al -Asp sample are presented in **Figure 5**. The cell parameters determined are reported in **Table 1** along with the values calculated from the simulations. The basal d -spacing is influenced by the interlayer water content. When the sample is fully dehydrated, the basal d -spacing was found to be 8.76 Å, which is slightly greater than the theoretically determined value of 7.73 Å. The orientation of the amino acid with respect to the LDH sheets can be estimated using simple geometry, as well as with computational chemistry methods, *vide infra*, based on the aspartate long-axis dimension being 6.8 Å (calculated with Chemwindow 6.0). In Scheme 1 an angle of 0° relative to the LDH layer sheet corresponds to a vertical orientation of the amino acid, and 90° to a vertical orientation. Extrapolating, the experimental data infers an angle of 36° relative to the sheet, compared with the c value of 26°.

When water entered the interlayer domain, higher order basal reflections were observed, suggesting a certain degree of order along the c direction. The d -spacing increases to 12.01 Å when the interlayer domain was fully hydrated, implying a vertical orientation of the intercalated amino acid. Although the trend of increasing d -spacing (and hence crystallographic c parameter) with increasing hydration was identifiable in the simulations, the increase was not as large as that observed experimentally.

This discrepancy between simulation and experiment is not unexpected, and is due to an artefact of the periodic DFT modelling method, namely artificial electrostatic interactions between the layers that are insufficiently screened by the interlayer species. Across the surface of each layer of the model double hydroxide, the electron density varies according to

the atomic structure, and when these layers are placed opposite to one another and separated by a vacuum there arise both Coulomb repulsions and dipolar attractions between the separated layers. Lennard-Jones described the electrostatics of surfaces in 1928 (Lennard-Jones and Dent, 1928), and they have since become well-known artefacts that occur when modelling periodic systems (Geatches, 2011). Molecules placed into the interlayer effectively screen the Coulomb repulsions, as indeed they do in the physical samples, but the dipole attraction in the models remains somewhat undiminished, and creates an electrostatic field between the layers, which affects the alignment of the interlayer molecules. In order to completely negate this effect, which is solely due to the modelled electron density, further screening between the layers (e.g. by the presence of more water molecules) would be required.

Important changes in the intensities of the XRD lines can also be noted when the hydration increases. From a crystallographic point of view in the hexagonal system, the (003) reflection corresponds to the plane of cations and the (006) plane corresponds to the plane located in the middle of the interlayer domain. Since the intensity of the XRD lines is proportional to the electron density along these planes, a more complete description of the interlayer organisation is gained by examining the evolution of the ratio $I(003)/I(006)$. Both the amino acid orientation and the location of the water molecules contribute to the electronic density along the different planes. A precise description of the structure of the interlayer water is thus possible only if the orientation of the amino acid is conserved. In the case where changes in orientations of the amino acid are observed on addition of water molecules, no detailed description can be carried out. This is the case when comparing the dehydrated sample with the samples containing 2 water molecules per aspartate. As deduced above from the analysis of the basal spacing, the orientation of the amino acid changes from a horizontal orientation to a vertical orientation. The increase of the $I(003)/I(006)$ ratio can be therefore

attributed to the decrease in electron density in the (006) plane as a result of the lower electron density of the vertical amino acids. Such a scenario prevents a precise description of the position of the water molecules. However, when the hydration reaches 10 water molecules per aspartate, the orientation of the amino acid remains vertical, so that the only change in electron density along the planes comes from the water molecules. A strong increase of the I(003)/I(006) ratio strongly suggests that the water molecules orientate from the middle of the interlayer, strongly interacting with both the carboxylate groups or amino group of the amino acids and the hydroxyl groups of the layers. The same behaviour was also observed in the DFT simulations.

The FTIR spectra give further insight into the intra- and intermolecular interactions of the amino acid. Changes in the stretching frequency of the anti-symmetric and symmetric modes of the carboxylate groups ($\Delta\nu = \nu_{as} - \nu_s$) can be indicators of the binding configuration (Greiner *et al.*, 2014; Roddick-Lanzilotta and McQuillan, 2000). The more asymmetric the interaction of the carbon-oxygen of the carboxylate group, the higher the difference in wave number between the anti-symmetric and symmetric stretching modes of the carboxylate. The general series $\Delta\nu_{unidentate} > \Delta\nu_{ionic} = \Delta\nu_{bridging} > \Delta\nu_{bidentate}$ was proposed and is supported by experimental work on metal chelate complexes. Given the LDH structure, it is unlikely that the amino acid would interact directly with the cations, but rather with the hydroxyl groups of the layer or with water molecules, if present, through hydrogen bonding, as observed in atomistic simulations by Kailinchev *et al.*, 2010. Moreover, the interlayer domain is dynamic and this results in different interlayer arrangements for a given basal spacing and water content, as evidenced by our computer simulations, *vide infra*. For all these reasons, the series above cannot be directly applied to our system with sufficient confidence.

As noted above, the aspartate solution for pH 11 gives a $\Delta\nu$ value of 164 cm⁻¹. Regardless of the water content, the $\Delta\nu$ for all three samples is in the range 155-183 cm⁻¹,

very close to that of the aqueous species. This suggests that aspartate interacts only weakly and mainly through hydrogen bonding. Such an interpretation is further supported by the almost constant intensity of the vibrational bands. The most notable difference is observed when varying the interlayer water content.

For the dehydrated sample, the interlayer *c*-dimension deduced from XRD analysis, implies that the amino acid is orientated horizontally within the interlayer domain. Such a configuration may favour either a bidentate (the two carboxylate oxygen interacting with one hydroxyl group from the layer) or a bridging configuration (one oxygen atom interacting with one hydroxyl from the upper layer, the other oxygen of the same carboxylate group interacting with a hydroxyl group from the lower layer). Since the vibrational peaks are much broader compared to those of aqueous aspartate, it is likely that both configurations are present in the interlayer domain, and indeed this is also reflected by the simulated model shown in **Figure 7a**. The observed $\Delta\nu$ was determined to be 183 cm^{-1} , slightly higher than that of the aqueous aspartate and may indicate a stronger bonding with the hydroxyl layer. When the sample was allowed to equilibrate with ambient relative humidity, the $\Delta\nu$ value shifted down to 165 cm^{-1} while the vibrational band become slightly narrower, although still broader than those of aqueous aspartate. This phenomenon may be related to the abrupt expansion of the interlayer spacing and subsequent re-organization of the interlayer amino acid. A bridging configuration of the amino acid is no longer possible, but a unidentate (one oxygen atom of the carboxylate group interacting with the hydroxyl layer, the other interacting with the interlayer species) or bidentate configuration remains plausible as illustrated by the DFT models presented in **Figure 7c**. However, since the structure of the interlayer domain is mainly governed by hydrogen bonding, these two configurations are expected to produce very similar $\Delta\nu$ and may explain the lower band broadness observed in the FTIR spectra. Further addition of water in the interlayer domain has no effect on the

stretching frequencies of the carboxylate group, thus indicating a similar bonding environment (as expected) since the basal spacings remain constant. The vibrational bands become narrower and are very comparable to those of aqueous aspartate. DFT models for the related structure also show that for such interlayer water content, the amino group can form hydrogen bonds to a LDH layer (**Figure 7c**). Further addition of water thus produces an isotropic bonding environment, with all carboxylate groups being involved in hydrogen bonding either with the hydroxyl layer or the water molecules.

Structure of Mg₃Al-Asp LDH. The Mg₃Al-Asp samples are different from the Mg₂Al-Asp samples. The XRD patterns and FTIR spectra of these samples for different relative humidity levels are displayed in **Figure 6**. Unlike the XRD pattern of the Mg₂Al-Asp samples, a good fit was obtained only if each XRD peak was split and fitted with two Lorentzians, suggesting the presence of materials with two different types of interlayer organizations. The dehydrated sample gives interlayer spacings of 8.44 Å and 7.89 Å that correspond to estimated aspartate orientations of 32° and 27° respectively with respect to the hydroxyl sheet (**Scheme 1** and **Table 2**), assuming a rigid aspartate molecule and the simulation studies reported here add further insight.

The simulated models for this system gave an interlayer spacing of 8.56 Å in good agreement with the experimental interlayer spacing. Negligible changes are observed when the Mg₃Al-Asp sample is equilibrated at 25% relative humidity, the interlayer spacing becoming 8.56 Å and 7.91 Å, which is very close to that of the dehydrated samples. The simulated interlayer spacings for these models give an average, depending on the starting configuration, value of 8.44 Å (DFT) and 8.40 Å for the MD simulation (**Table A4**), both are in good agreement with the experimental values. Note that the initial orientation of the amino acid in the DFT simulated structures has only a minor effect on the final, optimized

configurations, and the amino acid tends to be oriented with its long axis parallel to the layer (Figure 7). These results suggest that the layer charge density of the LDH affects the orientation of the amino acids at low hydration level. The experimental intensity ratio $I(003)/I(006)$ decreased when 2 water molecules per aspartate were added, which is correlated with the increase of the electronic density along the (006) plane where water molecules are more likely to be positioned given the restricted layer spacing, *vide supra*. A fully hydrated interlayer space gives experimental values of 11.06 Å and 11.80 Å, supporting a vertical orientation of the amino acid as was seen in the Mg₂Al-Asp sample. For the highest basal spacing (11.80 Å) the $I(003)/I(006)$ ratio (4.58) corresponds very closely with that experimentally determined for the highest basal spacing (12.01 Å) of the Mg₂Al-Asp (4.57) which means that a very similar interlayer organisation has taken place even if the quantity of interlayer water is slightly different (10 and 7 water molecules in the Mg₂Al-Asp and Mg₃Al-Asp structures respectively). While the orientation of the amino acid is governed mainly by the layer charge density, the interlayer water structure is ruled by the orientation of the amino acid.

The presence of the two interlayer structures at a given hydration state is also shown by analysis of the FTIR spectra. While the position of the stretching modes of the carboxylate groups is very comparable to those determined in the Mg₂Al-Asp sample, their width is obviously greater. The two interlayer structures are thus averaged in the FTIR spectra observed for the samples and this makes interpretation more complicated. Unfortunately, no obvious changes can be observed when varying the hydration, with the band position and width remaining similar. Based on the interpretation of the FTIR spectra on the Mg₂Al-Asp sample, and given the restricted interlayer spacing, low interlayer hydration would favour a bidentate or bridging configuration via hydrogen bonding (Figure 7d). In addition to the inherent difficulty provided by the two interlayer structures, a band located at 1360 cm⁻¹

assigned to the anti-symmetric stretching modes of carbonate is present. The carbonate LDH gives an interlayer spacing of around 7.8 Å and therefore should overlap with the XRD pattern of the phases with low levels of hydration. As demonstrated by Iyi *et al.* carbonate LDH does not exhibit any swelling properties, the interlayer spacing remaining unchanged whatever the relative humidity (Iyi *et al.*, 2007). Since no XRD lines corresponding to a basal spacing of 7.8 Å are observed in the fully hydrated phase, the presence of carbonate phases can be ruled out in our samples. Interestingly, the FTIR spectra of the fully hydrated sample present new vibrational bands located at 1320 and 1450 cm⁻¹ that were also found in the FTIR spectra of aqueous aspartate at pH 7 or 9. These two bands can therefore be assigned to the amino group in a protonated form. However, the stretching frequencies of the carboxylate groups do not present the characteristic shift in wavenumbers associated with the presence of the protonated amino group. This suggests that the aspartate is still charged -2 but with its amino group strongly involved in the hydrogen bonding network. Looking at the structures in **Figure 7e** and **7f**, it can be seen the amino group interacts more strongly with the hydroxyl layer when it is slightly tilted in the interlayer domain (**Figure 7e**) as compared with pure vertical orientation (**Figure 7f**).

5.3. Dynamics of the interlayer

Layered double hydroxides exist naturally, with a Mg₃Al-X structure being found in the commonest form of hydrotalcite. This Mg:Al ratio thus seems to be favoured in nature and should offer a greater stability than the Mg₂Al-X structure. This peculiarity may have been conserved throughout time, so that even on the early Earth, most of the compounds from the layered double hydroxides family may have been formed with the Mg₃Al-X structure. The interlayer structure of the Mg₃Al-Asp sample was thus further investigated by molecular dynamics at ambient conditions on large systems, allowing the sampling of numerous structures and their interactions with the inclusion of thermal motions. Such a study addresses

the question of whether or not the interlayer domain of LDHs can act as a template for the formation of peptides (Greenwell and Coveney, 2006).

MD analysis strongly supports our experimental data and enables further examination of the potential reactivity of the LDH phase toward the formation of peptides. In **Figure 11** we show the rapid increase in the potential reactive pairs, as the hydration drops below 5 waters per aspartate (totalling to 30% of all pairs). However, the interlayer domain does not present any regio-specificity since both α -peptide and β -peptide linkages are counted in similar quantities (~15%). It is likely that such selectivity is a matter of a reaction pathway and should be further studied with *ab initio* mechanistic methods. Our results demonstrate that peptide bond formation can occur in the interlayer domain of LDHs, and that it is more likely to occur in a dehydrated state than in aqueous solution, showing the potential importance of wetting/drying cycles.

6. Conclusions

We have examined the sorption of aspartate into layered double hydroxides. Our studies have shown that, contrary to previous studies (Aisawa *et al.*, 2004), it is possible to anion-exchange chloride-LDHs with amino acids at up to 100% of the anion exchange capacity by using alkaline pH conditions, giving an interlayer amino acid concentration of 7.93 mol/L starting from a very dilute solution (0.020 mol/L). Under geochemical conditions, it may be postulated that other anions may compete with the amino acids, though even at pH where considerable OH⁻ species are present, full exchange occurs. The strong affinity of LDH toward carbonate anions may restrict its anionic exchange capacity and the overall interlayer structure of the hybrid Mg_RAl-Asp system may be altered concomitantly. Therefore, in order to attain maximum adsorption and concentration of amino acids in layered minerals, the most plausible geochemical environments on the early Earth will be those with low dissolved CO₂

(and hence low carbonate), alkaline pH to ensure the amino acids are fully anionic and a pH gradient where layered hydroxide minerals precipitate. Such environments may have been low-medium temperature alkaline hydrothermal seeps, systems also suggested as providing chemical and energetic gradients by Russell and co-workers (Martin *et al.*, 2008; Martin and Russell, 2007; Russell *et al.*, 2013). The postulated abundance of LDHs on the early Earth suggests a route by which peptides may have formed abiotically.

In the present study, the potential for layered double hydroxide minerals to act as hosts for the concentration of the amino acid aspartate from solution has been studied, and the structure of the host-guest systems elucidated. Starting from $Mg_{1-x}Al_x(OH)_2Cl$ LDH, it was found that the chloride anions can be completely exchanged by aspartate anions at alkaline pH. The interlayer structures of the LDH-Asp containing various interlayer water contents were investigated by means of FTIR and XRD analysis coupled with electronic structure and atomistic computer simulations. As suggested by the adsorption isotherm, the interlayer aspartate molecules are present as dianions. The orientation of the amino acid within the interlayer is found to be mainly influenced by the layer charge density and to a lesser extent, by the interlayer water content, especially at high hydration levels. In general, low interlayer hydration produces a horizontal orientation of the amino acid, with the long axis being parallel to the layer, while high hydration levels induce a near-vertical orientation of the amino acid. For intermediate interlayer water contents, i.e. 2 water molecules per aspartate, it was observed that the layer charge density has a decisive role on the interlayer organisation, with a higher layer charge density inducing a more vertical orientation of the amino acid.

Molecular dynamic simulations of LDH show that peptide formation can occur in the interlayer domain of layered double hydroxides if the interlayer hydration is low, i.e. lower than 5 water molecules per aspartate anion. Future studies will explore whether amide bond formation can be attained without the need for heating, for example, through dehydrating

reagents such as carbonyl sulphide (COS) (Leman *et al.*, 2004) to illustrate that both concentrating and reaction mechanisms can occur at high pH in layered minerals, thus providing insight into whether low temperature alkaline seeps may have been plausible geochemical environments for abiotic peptide formation.

6. Acknowledgements

The authors wish to acknowledge the Leverhulme Foundation (VE, DGF, HCG, BG) for the funding that enabled this work. Computational resources were via HeCTOR (EPSRC EP/K013718/1). We wish to thank Professor Cedric Carteret for many useful discussions related to this work and HCG would like to thank Professor Gustaf Arrhenius for sharing his extensive knowledge and insight into this area, and the Royal Society for further funding. BG and DGF would like to thank Monica Price from the Oxford University Museum of Natural History and Phil Wiseman from the Chemistry Research Laboratory of the University of Oxford for giving access to FTIR and XRD facilities. VE would like to thank Matteo Degiacomi from Chemistry Research Laboratory of the University of Oxford for discussion and help in development of the analysis scripts.

844 References

- 845 Aimoz, L., Taviot-Guého, C., Churakov, S. V., Chukalina, M., Dähn, R., Curti, E., Bordet, P.,
846 and Vespa, M., (2012). Anion and Cation Order in Iodide-Bearing Mg/Zn–Al Layered
847 Double Hydroxides. *J. Phys. Chem. C* **116**, 5460-5475.
- 848 Aisawa, S., Kudo, H., Hoshi, T., Takahashi, S., Hirahara, H., Umetsu, Y., and Narita, E.,
849 (2004). Intercalation behavior of amino acids into Zn–Al-layered double hydroxide by
850 calcination–rehydration reaction. *J. Solid State Chem.* **177**, 3987-3994.
- 851 Arrhenius, G. O., (2003). Crystals and Life. *Helv. Chim. Acta* **86**, 1569-1586.
- 852 Baross, J. and Hoffman, S., (1985). Submarine hydrothermal vents and associated gradient
853 environments as sites for the origin and evolution of life. *Origins Life Evol. Biosphere*
854 **15**, 327-345.
- 855 Basiuk, V. A. and Sainz-Rojas, J., (2001). Catalysis of peptide formation by inorganic oxides:
856 High efficiency of alumina under mild conditions on the earth-like planets. *Adv. Space*
857 *Res.* **27**, 225-230.
- 858 Bellotto, M., Rebours, B., Clause, O., Lynch, J., Bazin, D., and Elkaïm, E., (1996). A
859 reexamination of hydrotalcite crystal chemistry *J. Phys. Chem.* **100**, 8527-8534.
- 860 Berendsen, H. J. C., Postma, J. P. M., van Gunsteren, W. F., and Hermans, J., (1981).
861 Interaction Models for Water in Relation to Protein Hydration. In: Pullman, B. (Ed.),
862 *Intermolecular Forces*. Springer Netherlands.
- 863 Bernal, J. D., (1949). The Physical Basis of Life. *Proceedings of the Physical Society. Section*
864 *B* **62**, 752.
- 865 Boulet, P., Greenwell, H. C., Stackhouse, S., and Coveney, P. V., (2006). Recent advances in
866 understanding the structure and reactivity of clays using electronic structure
867 calculations. *J. Mol. Struct.* **762**, 33-48.
- 868 Bujdák, J. and Rode, B. M., (1997). Silica, Alumina, and Clay-Catalyzed Alanine Peptide
869 Bond Formation. *J. Mol. Evol.* **45**, 457-466.
- 870 Bujdak, J., Slosiarikova, H., Texler, N., Schwendinger, M., and Rode, B. M., (1994). On the
871 possible role of montmorillonites in prebiotic peptide formation. *Monatshefte für*
872 *Chemie / Chemical Monthly* **125**, 1033-1039.
- 873 Chen, Q., Shi, S., Liu, X., Jin, L., and Wei, M., (2009). Studies on the oxidation reaction of l-
874 cysteine in a confined matrix of layered double hydroxides. *Chem. Eng. J.* **153**, 175-
875 182.
- 876 Clark, S. J., Segall, M. D., Pickard, C. J., Hasnip, P. J., Probert, M. I. J., Refson, K., and
877 Payne, M. C., (2005). First principles methods using CASTEP. *Zeitschrift für*
878 *Kristallographie* **220**, 567-570.
- 879 Coveney, P. V., Swadling, J. B., Wattis, J. A. D., and Greenwell, H. C., (2012). Theory,
880 modelling and simulation in origins of life studies. *Chem. Soc. Rev.* **41**, 5430-5446.
- 881 Cygan, R. T., Liang, J.-J., and Kalinichev, A. G., (2004). Molecular Models of Hydroxide,
882 Oxyhydroxide, and Clay Phases and the Development of a General Force Field. *The*
883 *Journal of Physical Chemistry B* **108**, 1255-1266.
- 884 Cygan, R. T., Liang, J.-J., and Kalinichev, A. G., (2004). Molecular Models of Hydroxide,
885 Oxyhydroxide, and Clay Phases and the Development of a General Force Field. *J.*
886 *Phys. Chem. B* **108**, 1255-1266.
- 887 Davidson, E. R. and Chakravorty, S., (1992). A test of the Hirshfeld definition of atomic
888 charges and moments. *Theor. Chim. Acta* **83**, 319-330.
- 889 Duan, X. and Evans, D. G., (2006). *Layered Double Hydroxides*. Springer.
- 890 Engel, M. H. and Nagy, B., (1982). Distribution and enantiomeric composition of amino acids
891 in the Murchison meteorite. *Nature* **296**, 837-840.
- 892 Ferris, J. P. and Hagan Jr, W. J., (1984). HCN and chemical evolution: The possible role of
893 cyano compounds in prebiotic synthesis. *Tetrahedron* **40**, 1093-1120.

894 Fitz, D., Reiner, H., and Rode, B. M., (2007). Chemical evolution toward the origin of life.
895 *Pure Appl. Chem.* **79**, 2101-2117.

896 Fraser, D. G., Fitz, D., Jakschitz, T., and Rode, B. M., (2011). Selective adsorption and chiral
897 amplification of amino acids in vermiculite clay-implications for the origin of
898 biochirality. *PCCP* **13**, 831-838.

899 Fraser, D. G., Greenwell, H. C., Skipper, N. T., Smalley, M. V., Wilkinson, M. A., Deme, B.,
900 and Heenan, R. K., (2011). Chiral interactions of histidine in a hydrated vermiculite
901 clay. *PCCP* **13**, 825-830.

902 Fudala, Á., Pálkó, I., and Kiricsi, I., (1999). Preparation and Characterization of Hybrid
903 Organic-Inorganic Composite Materials Using the Amphoteric Property of Amino
904 Acids: Amino Acid Intercalated Layered Double Hydroxide and Montmorillonite.
905 *Inorg. Chem.* **38**, 4653-4658.

906 Geatches, D., (2011). Clay minerals and their gallery guests. PhD thesis. Durham University.

907 Gilbert, W., (1986). Origin of life: The RNA world. *Nature* **319**, 618-618.

908 Greenwell, H. and Coveney, P. V., (2006). Layered Double Hydroxide Minerals as Possible
909 Prebiotic Information Storage and Transfer Compounds. *Origins Life Evol. Biosphere*
910 **36**, 13-37.

911 Greenwell, H. C., Jones, W., Coveney, P. V., and Stackhouse, S., (2006). On the application
912 of computer simulation techniques to anionic and cationic clays: A materials
913 chemistry perspective. *J. Mater. Chem.* **16**, 708.

914 Grégoire, B., Ruby, C., and Carteret, C., (2012). Structural Cohesion of MII-MIII Layered
915 Double Hydroxides Crystals: Electrostatic Forces and Cationic Polarizing Power.
916 *Cryst. Growth Des.* **12**, 4324-4333.

917 Greiner, E., Kumar, K., Sumit, M., Giuffrè, A., Zhao, W., Pedersen, J., and Sahai, N., (2014).
918 Adsorption of L-glutamic acid and L-aspartic acid to γ -Al₂O₃. *Geochim. Cosmochim.*
919 *Acta* **133**, 142-155.

920 Grimme, S., (2006). Semiempirical GGA-type density functional constructed with a long-
921 range dispersion correction. *J. Comput. Chem.* **27**, 1787-1799.

922 Hall, D. O., Cammack, R., and Rao, K. K., (1971). Role for Ferredoxins in the Origin of Life
923 and Biological Evolution. *Nature* **233**, 136-138.

924 Hanczyc, M. M., Fujikawa, S. M., and Szostak, J. W., (2003). Experimental Models of
925 Primitive Cellular Compartments: Encapsulation, Growth, and Division. *Science* **302**,
926 618-622.

927 Hashizume, H., Theng, B. K. G., and Yamagishi, A., (2002). Adsorption and discrimination
928 of alanine and alanyl-alanine enantiomers by allophane. *Clay Miner.* **37**, 551-557.

929 Hazen, R. M. and Sverjensky, D. A., (2010). Mineral Surfaces, Geochemical Complexities,
930 and the Origins of Life. *Cold Spring Harbor Perspectives in Biology* **2**.

931 Head, J. D. and Zerner, M. C., (1985). A Broyden-Fletcher-Goldfarb-Shanno optimization
932 procedure for molecular geometries. *Chem. Phys. Lett.* **122**, 264-270.

933 Hernandez, A. R. and Piccirilli, J. A., (2013). Chemical origins of life: Prebiotic RNA
934 unstuck. *Nat Chem* **5**, 360-362.

935 Hess, B., Kutzner, C., van der Spoel, D., and Lindahl, E., (2008). GROMACS 4: Algorithms
936 for Highly Efficient, Load-Balanced, and Scalable Molecular Simulation. *J. Chem.*
937 *Theory Comput.* **4**, 435-447.

938 Hibino, T., (2004). Delamination of Layered Double Hydroxides Containing Amino Acids.
939 *Chem. Mater.* **16**, 5482-5488.

940 Hines, D. R., Solin, S. A., Costantino, U., and Nocchetti, M., (2000). Physical properties of
941 fixed-charge layer double hydroxides. *Phys. Rev. B* **61**, 11348-11358.

942 Hofmeister, W. and Platen, H. V., (1992). Crystal Chemistry and Atomic Order in Brucite-
943 related Double-layer Structures. *Crystallogr. Rev.* **3**, 3-26.

944 Iyi, N., Fujii, K., Okamoto, K., and Sasaki, T., (2007). Factors influencing the hydration of
 945 layered double hydroxides (LDHs) and the appearance of an intermediate second
 946 staging phase. *Appl. Clay Sci.* **35**, 218-227.

947 Iyi, N., Yamada, H., and Sasaki, T., (2011). Deintercalation of carbonate ions from carbonate-
 948 type layered double hydroxides (LDHs) using acid-alcohol mixed solutions. *Appl.*
 949 *Clay Sci.* **54**, 132-137.

950 Kalinichev, A. G., Kumar, P. P., and Kirkpatrick, R. J., (2010). Molecular dynamics computer
 951 simulations of the effects of hydrogen bonding on the properties of layered double
 952 hydroxides intercalated with organic acids. *Philos. Mag.* **90**, 2475-2488.

953 Kelley, D. S., Karson, J. A., Blackman, D. K., Fruh-Green, G. L., Butterfield, D. A., Lilley,
 954 M. D., Olson, E. J., Schrenk, M. O., Roe, K. K., Lebon, G. T., Rivizzigno, P., and the,
 955 A. T. S. P., (2001). An off-axis hydrothermal vent field near the Mid-Atlantic Ridge at
 956 30[deg] N. *Nature* **412**, 145-149.

957 Kelley, D. S., Karson, J. A., Früh-Green, G. L., Yoerger, D. R., Shank, T. M., Butterfield, D.
 958 A., Hayes, J. M., Schrenk, M. O., Olson, E. J., Proskurowski, G., Jakuba, M., Bradley,
 959 A., Larson, B., Ludwig, K., Glickson, D., Buckman, K., Bradley, A. S., Brazelton, W.
 960 J., Roe, K., Elend, M. J., Delacour, A., Bernasconi, S. M., Lilley, M. D., Baross, J. A.,
 961 Summons, R. E., and Sylva, S. P., (2005). A Serpentinite-Hosted Ecosystem: The Lost
 962 City Hydrothermal Field. *Science* **307**, 1428-1434.

963 Kuma, K., Paplawsky, W., Gerdul, B., and Arrhenius, G., (1989). Mixed-valence hydroxides
 964 as bioorganic host minerals. *Origins Life Evol. Biosphere* **19**, 573-601.

965 Kumar, P. P., Kalinichev, A. G., and Kirkpatrick, R. J., (2006). Hydration, Swelling,
 966 Interlayer Structure, and Hydrogen Bonding in Organolayered Double Hydroxides:
 967 Insights from Molecular Dynamics Simulation of Citrate-Intercalated Hydrotalcite. *J.*
 968 *Phys. Chem. B.* **110**, 3841-3844.

969 Kumar, P. P., Kalinichev, A. G., and Kirkpatrick, R. J., (2007). Molecular Dynamics
 970 Simulation of the Energetics and Structure of Layered Double Hydroxides Intercalated
 971 with Carboxylic Acids. *J. Phys. Chem. C* **111**, 13517-13523.

972 Lambert, J.-F., (2008). Adsorption and Polymerization of Amino Acids on Mineral Surfaces:
 973 A Review. *Origins of Life and Evolution of Biospheres* **38**, 211-242.

974 Lang, S. Q., Butterfield, D. A., Schulte, M., Kelley, D. S., and Lilley, M. D., (2010). Elevated
 975 concentrations of formate, acetate and dissolved organic carbon found at the Lost City
 976 hydrothermal field. *Geochim. Cosmochim. Acta* **74**, 941-952.

977 Lascelles, D. F., (2007). Black smokers and density currents: A uniformitarian model for the
 978 genesis of banded iron-formations. *Ore Geology Reviews* **32**, 381-411.

979 Lee, M. H., (1996). PhD thesis. PhD Thesis. Cambridge University.

980 Leman, L., Orgel, L., and Ghadiri, M. R., (2004). Carbonyl Sulfide-Mediated Prebiotic
 981 Formation of Peptides. *Science* **306**, 283-286.

982 Lennard-Jones, J. E. and Dent, B. M., (1928). Cohesion at a crystal surface. *Trans. Faraday*
 983 *Soc.* **24**, 92-108.

984 MacKerell, A. D., Banavali, N., and Foloppe, N., (2000). Development and current status of
 985 the CHARMM force field for nucleic acids. *Biopolymers* **56**, 257-265.

986 Martin, R., (2004). *Electronic structure: basic theory and practical methods*. Cambridge
 987 University Press.

988 Martin, W., Baross, J., Kelley, D., and Russell, M. J., (2008). Hydrothermal vents and the
 989 origin of life. *Nat. Rev. Microbiol.* **6**, 805-814.

990 Martin, W. and Russell, M. J., (2007). On the origin of biochemistry at an alkaline
 991 hydrothermal vent. *Philos. T. Roy. Soc. B* **362**, 1887-1925.

992 Martra, G., Deiana, C., Sakhno, Y., Barberis, I., Fabbiani, M., Pazzi, M., and Vincenti, M.,
 993 (2014). The Formation and Self-Assembly of Long Prebiotic Oligomers Produced by

994 the Condensation of Unactivated Amino Acids on Oxide Surfaces. *Angew. Chem. Int.*
 995 *Ed.* **53**, 4671-4674.
 996 McNellis, E. R., Meyer, J., and Reuter, K., (2009). Azobenzene at coinage metal surfaces:
 997 Role of dispersive van der Waals interactions. *Phys. Rev. B: Condens. Matter* **80**.
 998 Mejias, J. A., Berry, A. J., Refson, K., and Fraser, D. G., (1999). The kinetics and mechanism
 999 of MgO dissolution. *Chem. Phys. Lett.* **314**, 558-563.
 1000 Monkhorst, H. J. and Pack, J. D., (1976). Special points for Brillouin-zone integrations. *Phys.*
 1001 *Rev. B* **13**, 5188-5192.
 1002 Mulliken, R. S., (1955). Electronic population analysis on LCAO-MO molecular wave
 1003 functions. I. *J. Chem. Phys.* **23**, 1833-1840.
 1004 Mulliken, R. S., (1955). Electronic population analysis on LCAO-MO molecular wave
 1005 functions. II. Overlap populations, bond orders, and covalent bond energies. *J. Chem.*
 1006 *Phys.* **23**, 1841-1846.
 1007 Mulliken, R. S., (1955). Electronic population analysis on LCAO-MO molecular wave
 1008 functions. III. effects of hybridization on overlap and gross AO populations. *J. Chem.*
 1009 *Phys.* **23**, 2338-2342.
 1010 Mulliken, R. S., (1955). Electronic population analysis on LCAO-MO molecular wave
 1011 functions. IV. bonding and antibonding in LCAO and valence-bond theories. *J. Chem.*
 1012 *Phys.* **23**, 2343-2346.
 1013 Newman, S. P., Williams, S. J., Coveney, P. V., and Jones, W., (1998). Interlayer
 1014 Arrangement of Hydrated MgAl Layered Double Hydroxides Containing Guest
 1015 Terephthalate Anions: Comparison of Simulation and Measurement. *J. Phys. Chem. B*
 1016 **102**, 6710-6719.
 1017 Pálincó, I., (2006). Organic-Inorganic Nanohybrids of Biologically Important Molecules and
 1018 Layered Double Hydroxides. *Nanopages* **1**, 295-314.
 1019 Patel, B. H., Percivalle, C., Ritson, D. J., DuffyColm, D., and Sutherland, J. D., (2015).
 1020 Common origins of RNA, protein and lipid precursors in a cyanosulfidic
 1021 protometabolism. *Nat Chem* **7**, 301-307.
 1022 Perdew, J. P., Burke, K., and Ernzerhof, M., (1996). Generalized gradient approximation
 1023 made simple. *Phys. Rev. Lett.* **77**, 3865-3868.
 1024 Pisson, J., Morel-Desrosiers, N., Morel, J. P., de Roy, A., Leroux, F., Taviot-Guého, C., and
 1025 Malfreyt, P., (2011). Tracking the Structural Dynamics of Hybrid Layered Double
 1026 Hydroxides. *Chem. Mater.* **23**, 1482-1490.
 1027 Plankensteiner, K., Righi, A., Rode, B. M., Gargallo, R., Jaumot, J., and Tauler, R., (2004).
 1028 Indications towards a stereoselectivity of the salt-induced peptide formation reaction.
 1029 *Inorg. Chim. Acta* **357**, 649-656.
 1030 Powner, M. W., Gerland, B., and Sutherland, J. D., (2009). Synthesis of activated pyrimidine
 1031 ribonucleotides in prebiotically plausible conditions. *Nature* **459**, 239-242.
 1032 Reinholdt, M. X., Babu, P. K., and Kirkpatrick, R. J., (2009). Preferential Adsorption of
 1033 Lower-Charge Glutamate Ions on Layered Double Hydroxides: An NMR
 1034 Investigation. *J. Phys. Chem. C* **113**, 3378-3381.
 1035 Richardson, I. G., (2013). The importance of proper crystal-chemical and geometrical
 1036 reasoning demonstrated using layered single and double hydroxides. *Acta Crystallogr.*
 1037 *Sect. B: Struct. Sci.* **69**, 150-162.
 1038 Rimola, A., Sodupe, M., and Ugliengo, P., (2007). Aluminosilicate Surfaces as Promoters for
 1039 Peptide Bond Formation: An Assessment of Bernal's Hypothesis by ab Initio
 1040 Methods. *J. Am. Chem. Soc.* **129**, 8333-8344.
 1041 Roddick-Lanzilotta, A. D. and McQuillan, A. J., (2000). An in situ Infrared Spectroscopic
 1042 Study of Glutamic Acid and of Aspartic Acid Adsorbed on TiO₂: Implications for the
 1043 Biocompatibility of Titanium. *J. Colloid Interface Sci.* **227**, 48-54.

- Rode , B. M., (1999). Peptides and the origin of life. *Peptides* **20**, 773-786.
- Russell, M. J., (2003). The Importance of Being Alkaline. *Science* **302**, 580-581.
- Russell, M. J., Nitschke, W., and Branscomb, E., (2013). The inevitable journey to being. *Philos. T. Roy. Soc. B* **368**.
- Sanchez-Portal, D., Artacho, E., and Soler, J. M., (1995). Projection of plane-wave calculations into atomic orbitals. *Solid State Commun.* **95**, 685-690.
- Schoonen, M., Smirnov, A., and Cohn, C., (2004). A Perspective on the Role of Minerals in Prebiotic Synthesis. *J. Hum. Environ. Syst* **33**, 539-551.
- Schwendinger, M. G. and Rode, B. M., (1992). Investigations on the mechanism of the salt-induced peptide formation. *Origins Life Evol. Biosphere* **22**, 349-359.
- Segall, M. D., Pickard, C. J., Shah, R., and Payne, M. C., (1996). Population analysis in plane wave electronic structure calculations. *Mol. Phys.* **89**, 571-577.
- Segall, M. D., Shah, R., Pickard, C. J., and Payne, M. C., (1996). Population analysis of plane-wave electronic structure calculations of bulk materials. *Phys. Rev. B: Condens. Matter* **54**, 16317-16320.
- Sleep, N. H., (2010). The Hadean-Archaeon Environment. *Cold Spring Harbor Perspectives in Biology* **2**.
- Thyveetil, M.-A., Coveney, P. V., Suter, J. L., and Greenwell, H. C., (2007). Emergence of Undulations and Determination of Materials Properties in Large-Scale Molecular Dynamics Simulation of Layered Double Hydroxides. *Chem. Mater.* **19**, 5510-5523.
- Trave, A., Selloni, A., Goursot, A., Tichit, D., and Weber, J., (2002). First Principles Study of the Structure and Chemistry of Mg-Based Hydrotalcite-Like Anionic Clays. *J. Phys. Chem. B* **106**, 12291-12296.
- Ugliengo, P., Zicovich-Wilson, C. M., Tosoni, S., and Civalleri, B., (2009). Role of dispersive interactions in layered materials: A periodic B3LYP and B3LYP-D* study of Mg(OH)₂, Ca(OH)₂ and kaolinite. *J. Mater. Chem.* **19**, 2564-2572.
- Underwood, T., Erastova, V., Cubillas, P., and Greenwell, H. C., (2015). Molecular Dynamic Simulations of Montmorillonite–Organic Interactions under Varying Salinity: An Insight into Enhanced Oil Recovery. *J. Phys. Chem. C*.
- Vanderbilt, D., (1990). Soft self-consistent pseudopotentials in a generalized eigenvalue formalism. *Phys. Rev. B* **41**, 7892-7895.
- Wei, M., Yuan, Q., Evans, D. G., Wang, Z., and Duan, X., (2005). Layered solids as a "molecular container" for pharmaceutical agents: l-tyrosine-intercalated layered double hydroxides. *J. Mater. Chem.* **15**, 1197-1203.
- Whilton, N. T., Vickers, P. J., and Mann, S., (1997). Bioinorganic clays: synthesis and characterization of amino- and polyamino acid intercalated layered double hydroxides. *J. Mater. Chem.* **7**, 1623-1629.
- Wolpert, M. and Hellwig, P., (2006). Infrared spectra and molar absorption coefficients of the 20 alpha amino acids in aqueous solutions in the spectral range from 1800 to 500 cm⁻¹. *Spectrochim. Acta A* **64**, 987-1001.

Tables

Insights into the Behaviour of Biomolecules on the Early Earth: The Concentration of Aspartate by Layered Double Hydroxide Minerals

Brian Grégoire^a, Valentina Erastova^b, Dawn L. Geatches^c, Stewart J. Clark^d, H. Christopher Greenwell^{b*}, Donald G. Fraser^a.

^aDepartment of Earth Sciences, University of Oxford, South Parks Road, Oxford, OX1 3AN, UK

^bDepartment of Earth Sciences, Durham University, South Road, Durham, DH1 3LE, UK

^c Daresbury Laboratory (STFC), Warrington, WA4 4AD, UK

^dDepartment of Physics, Durham University, South Road, Durham, DH1 3LE, UK

Table captions

Table 1: Experimental cell parameters, XRD intensity ratio and orientation angle of aspartate with respect to the hydroxyl surface along with the calculated values from DFT models with different interlayer water content in $\text{Mg}_2\text{Al-Asp}$.

Table 2 : Experimental cell parameters, XRD intensity ratio and orientation angle of aspartate with respect to the hydroxyl surface along with the calculated values from DFT and MD models with different interlayer water content in $\text{Mg}_3\text{Al-Asp}$.

Table 1

Mg ₂ Al-Asp H ₂ O/Asp	c ₀ param (Å)	c param (Å)	I ₀₀₃ /I ₀₀₆	Angle Θ _{exp} (°)	Calc. value (Å)	Angle Θ _{th} (°)
0 (Mg ₂ AlOH ₆ Asp _{1/2})	26.29	8.76	1,52	54	7.73	65
2 (Mg ₂ AlOH ₆ Asp _{1/2} . 1H ₂ O)	35.89	11.96	2.00	0	8.27	59
5 (Mg ₂ AlOH ₆ Asp _{1/2} . 2.5H ₂ O)	NA	NA	NA	NA	9.6 ⁽¹⁾	45
7 (Mg ₂ AlOH ₆ Asp _{1/2} . 3.5H ₂ O)	36.03	12.01	4.57	0	NA	NA

Table 2

Mg ₃ Al-Asp H ₂ O/Asp	c ₀ param (Å)	c param (Å)	I ₀₀₃ /I ₀₀₆	Angle Θ_{exp} (°)	Calc. value (Å)	Angle Θ_{th} (°)
0 (Mg ₃ AlOH ₈ Asp _{1/2})	23.67 25.32	7.89 8.44	1.78 1.77	63 58	7.73 ^[DFT] 8.4 ^[MD]	65
2 (Mg ₃ AlOH ₈ Asp _{1/2} . 1H ₂ O)	23.72 25.69	7.91 8.56	1.24 0.85	63 56	8.00 ^{[DFT] (1)} 8.75 ^{[DFT] (1)} 8.40 ^[MD]	62 55
5 (Mg ₃ AlOH ₈ Asp _{1/2} . 2.5H ₂ O)	N.A	N.A	N.A	N.A	9.53 ^{[DFT] (1)} 10.98 ^{[DFT] (1)}	46 25
10 (Mg ₂ AlOH ₆ Asp _{1/2} . 5H ₂ O)	33.17 35.39	11.06 11.80	3.24 4.58	23 0	10.65 ^{[MD] (3)}	

(1) The two calculated basal spacing corresponds to the extreme values of the simulation cells starting with aspartate in different orientation

(2) Extracted from MD simulation on Mg₃AlOH₈Asp_{1/2}.5H₂O

Scheme

Insights into the Behaviour of Biomolecules on the Early Earth: The Concentration of Aspartate by Layered Double Hydroxide Minerals

Brian Grégoire^a, Valentina Erastova^b, Dawn L. Geatches^c, Stewart J. Clark^d, H. Christopher Greenwell^{b*}, Donald G. Fraser^a.

^aDepartment of Earth Sciences, University of Oxford, South Parks Road, Oxford, OX1 3AN, UK

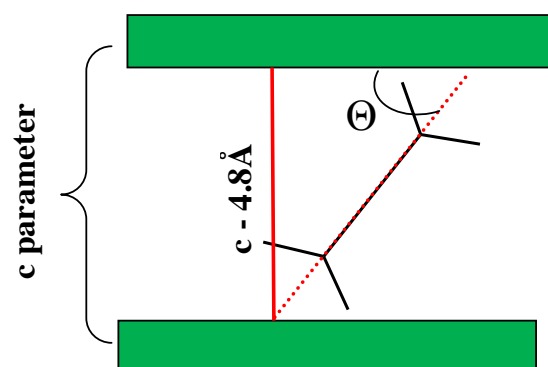
^bDepartment of Earth Sciences, Durham University, South Road, Durham, DH1 3LE, UK

^cDaresbury Laboratory (STFC), Warrington, WA4 4AD, UK

^dDepartment of Physics, Durham University, South Road, Durham, DH1 3LE, UK

Scheme caption

Scheme 1: Estimation of the tilt angle (Θ) of the interlayer aspartate amino acid based on the experimental c parameters.



Scheme 1

Figures

Insights into the Behaviour of Biomolecules on the Early Earth: The Concentration of Aspartate by Layered Double Hydroxide Minerals

Brian Grégoire^a, Valentina Erastova^b, Dawn L. Geatches^c, Stewart J. Clark^d, H. Christopher Greenwell^{b*}, Donald G. Fraser^a.

^aDepartment of Earth Sciences, University of Oxford, South Parks Road, Oxford, OX1 3AN, UK

^bDepartment of Earth Sciences, Durham University, South Road, Durham, DH1 3LE, UK

^c Daresbury Laboratory (STFC), Warrington, WA4 4AD, UK

^dDepartment of Physics, Durham University, South Road, Durham, DH1 3LE, UK

Figures captions

Figure 1. A schematic to show the general structure of a layered double hydroxide mineral, illustrating how one set of interlayer anions may be exchanged for another, with the two-dimensional layered structure adapting to the increased size of the new guest molecule. The colour scheme is M^{3+} = dark grey; M^{2+} = green; O = red; N = blue; C = middle grey; H = white; Cl = pink.

Figure 2. Powder X-ray diffraction patterns for (a) Mg_2Al-X , and (b) Mg_3Al-X layered double hydroxide materials prepared, with the corresponding infra-red spectra, (c) for Mg_2Al-X , and (d) Mg_3Al-X . Where X = CO_3 or Cl.

Figure 3. Adsorption isotherms of aspartate for: (a) Mg_2Al-Cl , and (b) Mg_3Al-Cl . The plots show that at both Mg/Al ratios, the maximum adsorption capacity is around 1 aspartate per 2 Al, confirming aspartate is present as the doubly charged (2-) form.

Figure 4. ATR-FTIR spectra of (a) aspartate solution ($[Asp] = 1M$) at pH 7, 9 and 11 and (b) colloidal suspension of aspartate intercalated into the interlayer domain of 2:1 LDH at pH 9 and 11.

Figure 5. On the left the powder X-Ray diffraction patterns of $Mg_2Al-Asp$ are shown at different interlayer water content. The right hand side shows the FTIR spectra of the same materials (Samples obtained from $[Asp]_0 = 50\text{ mM}$; pH = 11; Contact time = 20 h)

Figure 6. On the left the powder X-Ray diffraction patterns of $Mg_3Al-Asp$ are shown at different interlayer water content. The right hand side shows the FTIR spectra of the same materials (Samples obtained from $[Asp]_0 = 50\text{ mM}$; pH = 11; Contact time = 20 h)

Figure 7. DFT optimised $Mg_2Al-Asp$ (a-c) and $Mg_3Al-Asp$ (d-f) structures containing (a,d) 0 water molecule per aspartate, (b,e) 2 water molecules per aspartate and (c,f) 5 water molecules per aspartate

Figure 8. Side view of a slice of the MD simulation box of LDH31 with charge balancing aspartate 2- and varying amounts of water: (a) 20 water molecules per aspartate, (b) 15 water molecules per aspartate, (c) 10 water molecules per aspartate, (d) 7 water molecules per aspartate, (e) 5 water molecules per aspartate, (f) 3 water molecules per aspartate, (g) 2 water molecules per aspartate and (h) no water. LDH31 is shown as VDW spheres, where pink is Mg, cyan is Al, red is O and white is H; Aspartate is shown as thick liquorice, where cyan is C, blue is N, red is O and white is H, water is shown as thin liquorice, where red is O and white is H. The top and bottom clay layer are given fully, while being a periodic copy.

Figure 9. The figures show alignment of the vector between (a) two oxygens of carboxyl group on side chain; (b) two oxygens on carboxyl group of the back bone; (c) between two carbons of the carboxyl group, the schematic vector assignment is given in (d). The angle is given with respect to the LDH layer. The colours are per system: 0 water system – red, 2 waters per aspartate – orange, 3 waters per aspartate – lime, 5 waters per aspartate – green, 7 waters per aspartate – light blue, 10 waters per aspartate – blue, 15 waters per aspartate – purple, 20 waters per aspartate – magenta.

Figure 10. possible reactive alignments of aspartate leading to (a) alpha-peptide, (b) beta-peptide and (c) cyclic structure that would prevent beta-peptide formation.

Figure 11. Expected quantity of peptides formed (%) within the interlayer gallery of LDH with various interlayer water content.

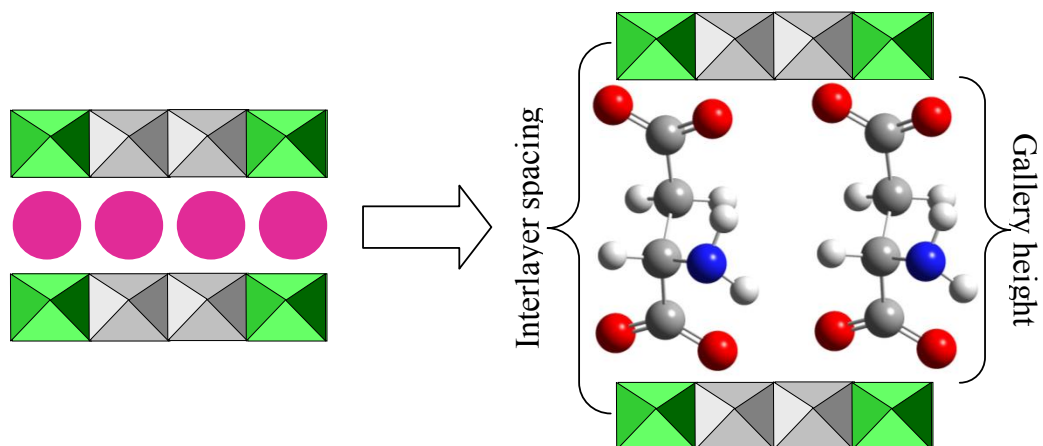


Figure 2

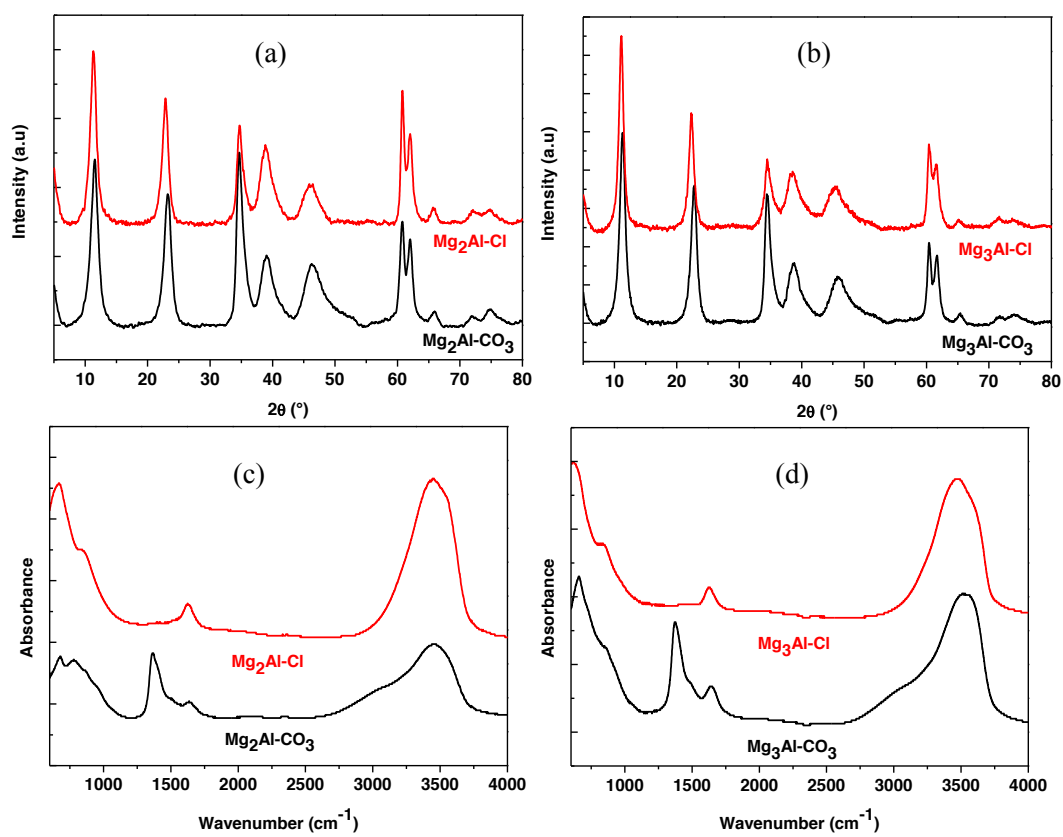


Figure 2

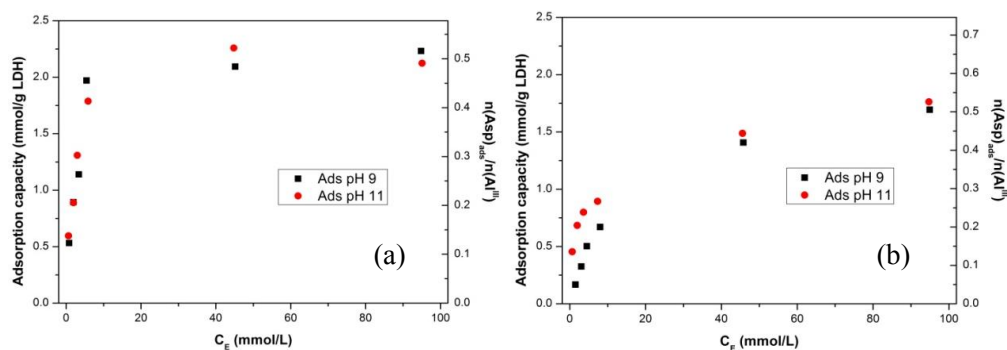


Figure 3

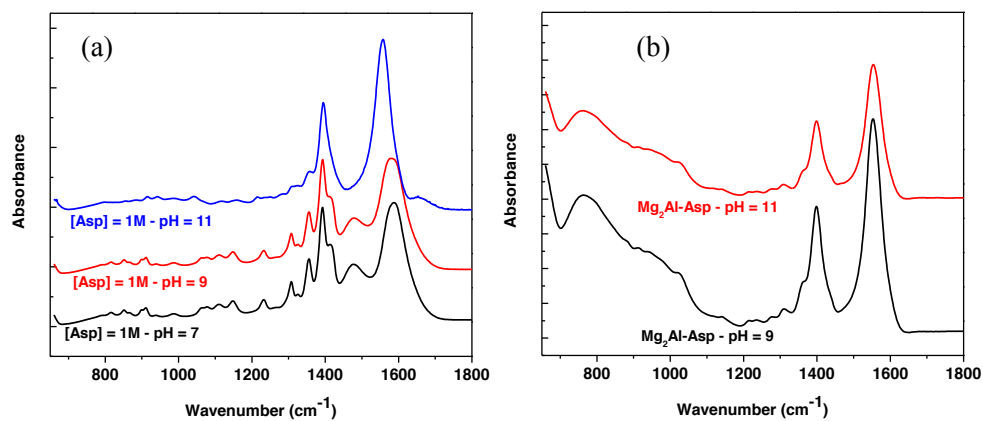


Figure 4

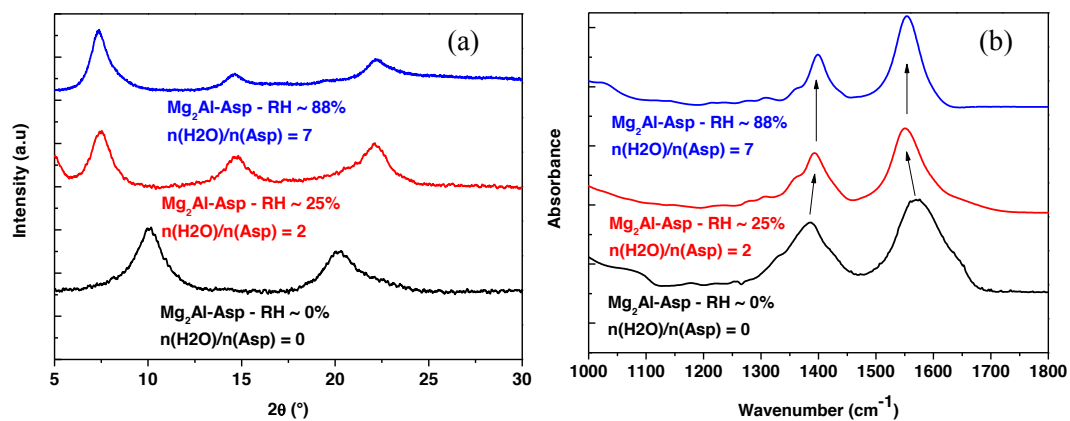


Figure 5

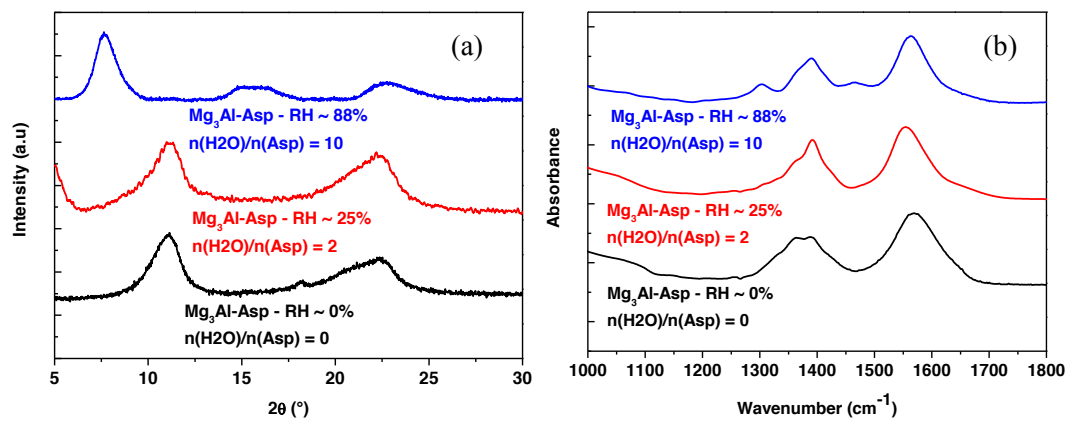


Figure 6

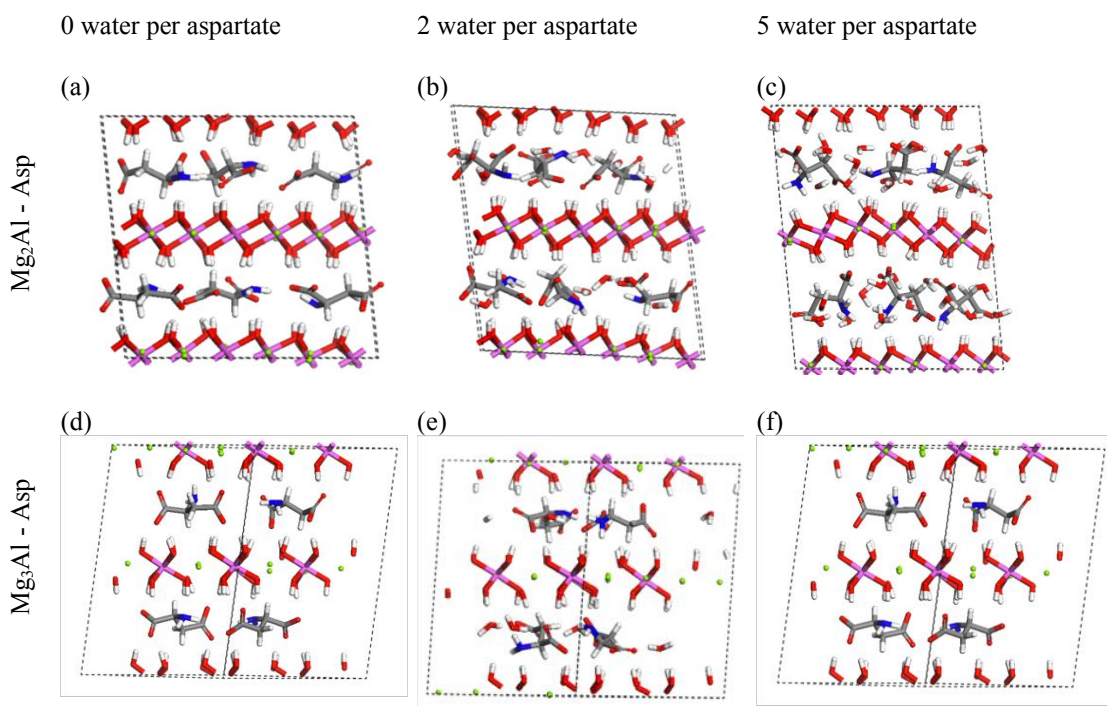


Figure 7

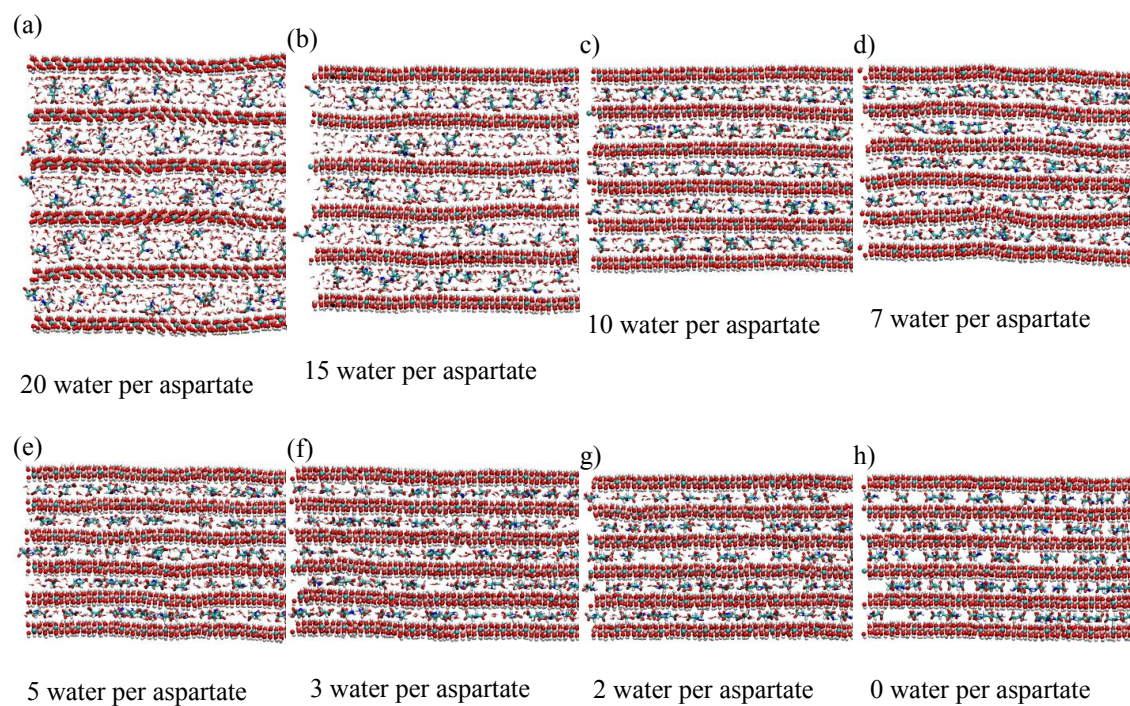


Figure 8

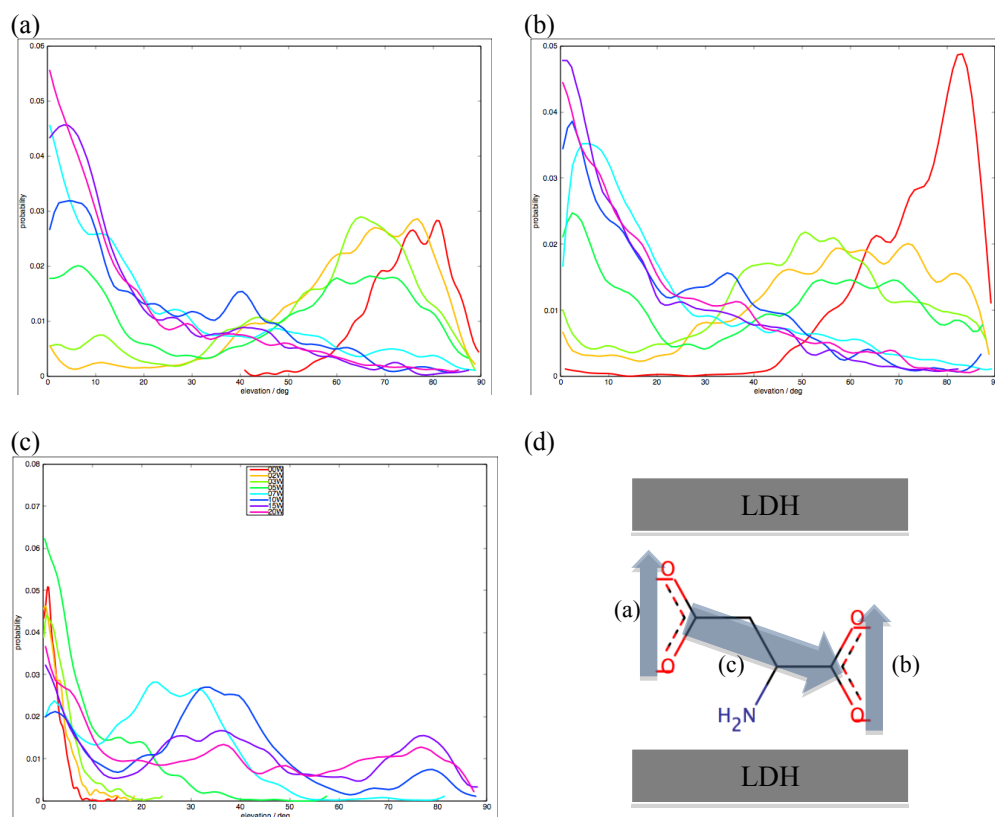


Figure 9

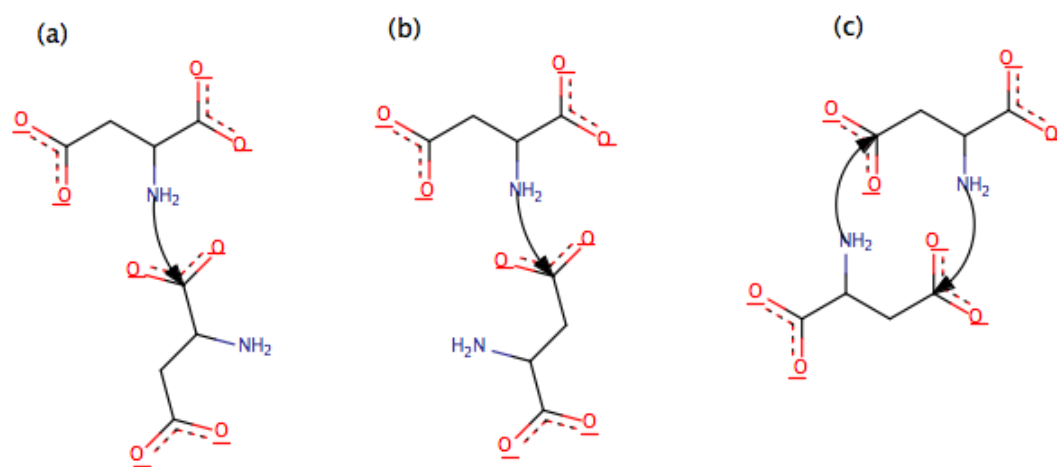


Figure 10

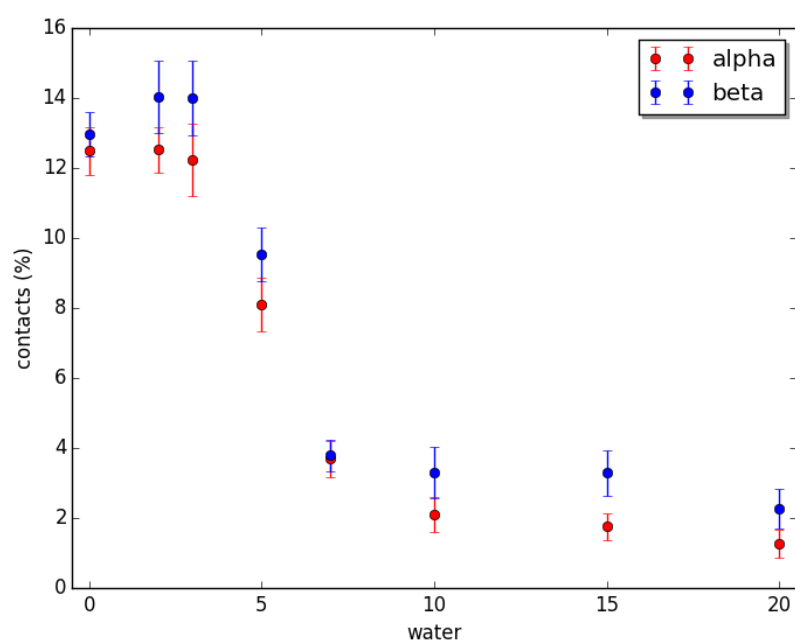


Figure 11

Appendix

[Click here to download Appendix: Appendix A.docx](#)